Implementing active control to reduce the response amplification of transition zones in railway tracks

A theoretical investigation

Tomas Andres Ramirez

Thesis Committee:
Asst. Prof. Karel van Dalen (Chair)
Prof. Andrei Metrikine
Dr. Andrei Faragau
Ir. Avni Jain

September 2023

Delft University of Technology

Civil Engineering department

Abstract

The maintenance and repairs of transition zones pose significant challenges in the railways industry due to their accelerated degradation rates in comparison to free tracks. These zones, characterized by track property variations, amplify their response when a source travels along the tracks. The resulting amplifications in stress and strain fields lead to differential settlements, affecting both track's stability and passenger comfort. This study investigates the influence of incorporating active control forces and moments at the interface of transition zones to mitigate the excessive degradation of soft domains.

Three 1-dimensional models are developed, which include active control forces and moments as a novel method to minimize the amplification of the response in the soft domain of transition zones, as well as, the derivation of these forces. The purpose of these three models is to give the reader an inside view of the method to derive these active control forces with models that increase in complexity.

The first model involves an Euler-Bernoulli beam resting on a piece-wise inhomogeneous Winkler foundation. The second model extends this by including a shear beam and a second layer of foundation, with the first layer being homogeneous and the second layer piece-wise inhomogeneous (Kerr foundation). The third model is a hybrid model between the first two, on which the soft domain is represented by the description of the second model, and the rigid domain by the description of the first model. Numerical solutions in the time-domain were applied to these models, and the study focused on a transition zone subjected to a constant amplitude moving load with constant velocity, traveling from a soft to stiff domain. The purpose of the first model is to give the reader a general idea on the derivation of a very simplistic model. The second model's purpose is to better represent the different elements of a railway structure, on which the shear beam and the lower layer of springs represent the mobilised soil under the tracks, while the top layer of springs and the Euler-Bernoulli beam represent the ballast, the sleepers and the rail. Finally, the third model was made to represent a transition zones, on which the soil is discontinued due to a man-made structure, e.g. a concrete bridge, which leads the structure under the ballast, in the rigid domain, to be consider infinitely stiff and to be represented just by an Euler-Bernoulli beam on a Winkler foundation.

Findings reveal that the active control forces and moments are capable of fully mitigating the dynamic amplification in soft domains of transition zones, however, they increase the dynamic amplifications in the stiff domain. Moreover, the shape that these forces take over time is dictated by the interaction between both domains of the transition zone, when the interface of the transition zone has continuous elements, the forces take a similar shape to the eigenfield of the system, while when there is discontinuous elements over the interface, the forces take a 'flipping' shape. Furthermore, of the two parameters studied (velocity of the moving load and vertical stiffness), the

dominating parameter in the response of the system depends upon the regime that the system is being subjected to. For relatively low and extremely high velocities of the moving load, the system is dominated by the vertical stiffness ratio, while for medium velocities of the moving load, the system is dominated by the velocity of the moving load. Finally, transition zones with discontinuous elements require significantly more energy to be absorbed and added into the system by the active control forces to mitigate the dynamic amplifications in the soft domain of the system.

These thesis offer valuable insights for preliminary designs of active control forces aimed at diminishing the dynamic amplification of soft domains of transition zones railway.

Acknowledgements

I want to thanks my parents Lucia Cecilia Margozzini Guglielmetti and Rodrigo Osvaldo Ramirez Cardenas, who unconditionally supported me through my studies, and for all the sacrifices that they had to make for me to continue my path. I can finally tell them that their efforts were not in vain, and that finally the cycle is over. To my sister Lucia Eugenia Ramirez Margozzini who kept motivating me to continue without giving up. To my brother Rodrigo Arquimedes Ramirez Margozzini, without him none of my accomplishment were to have been possible, as he was the person who convinced me to pursue this path.

To Maximiliano Eduardo Ojeda Aguila and Ian Kev Phillips Richardson my best friends in life. Even though we have chosen quite different paths, with each year, our bond grows stronger. You have been my welcomed distraction from the struggles of studying, bringing joy and perspective to every chapter of this academic journey. Your friendship is a cherished gift I carry with gratitude.

To my beloved girlfriend, Camille Pernollet, she is the person who has seen everything first handed. Your patience, understanding, and belief in me have been my driving force. Your encouragement during the late nights of studying, your gentle reassurance during moments of self-doubt, and your warm presence in celebrating even the smallest victories have made this journey not only bearable but beautiful.

My gratitude expands to all the people aforementioned. Without them, I would not have finished my degree. Each individual contributed towards this process in their own way. The least I can do is to immortalise my gratitude by commemorating you in these acknowledgements,

With enduring appreciation,
Tomas Andres Ramirez Margozzini

Contents

List of Figures

List of Tables

Chapter 1

Introduction

1.1 Background Information

Railways have been used for centuries all around the world to transport people and goods. With globalization and the development of countries, more tracks are being placed to reach already existing, and new destinations in a quicker and more efficient manner. As a consequence, every year there is more of the railway systems to maintain and repair. During the construction of railway tracks, as the rails are advancing, obstacles must be overcome to reach the destinations. Because of these obstacles, (e.g. rivers, mountains, canals, etc.), manmade structures must be built for the tracks to continue. For instance, bridges to cross over rivers, or tunnels to go through mountains.

The zones around the interface of these manmade structures and the pre-existing natural structures, are called "transition zones". These zones are of particular importance to the railway industry; they tend to exhibit a higher degradation and deterioration rate compared to tracks afar from these zones (also known as "free tracks"). In fact, according to Meijers and Hölscher [20], transition zones require 2 to 4 times more maintenance than the "free" track.

Moreover, according to the European Commission [6], €38.7 billion were spent in rail infrastructure by the European Member States (EU27) just in 2018. About 55% of this money (€21.3 billion) was spent only on renewals and maintenance, while only 20% of the money (€8 billion) in new infrastructure.

This evidences the great saving potential that can be made, if the frequency of renewals and maintenance of railways were to decrease. Specially as maintenance of tracks disrupts the normal traffic of the railway system, often causing delays or cancelling of trains. However, for this to happen significant improvements in the understanding on the behaviour of the accelerated degradation of transition zones must be achieved.

1.2 Objectives of this Study and Research Question

The problem in transition zones arises when a train travels from or towards a stiffer structure, such as a bridge, and an abrupt change in the stiffness of the system occurs. This increases the loading of the different components of the tracks and in the soil underneath, increasing the deterioration rate of the tracks.

According to Paixao et al. [23], there are two main factors of problems at transition zones:

1. The abrupt variation of the track's vertical stiffness due to different support conditions. For instance, less stiffness over earthworks, while higher stiffness on bridges or culverts, and
2. The differential settlement between the structure and the backfilling of the abutment.

Furthermore, they (Paixao et al.) stated that these two factors severely amplify the dynamic train-track interaction if the transition zone is not properly designed and/or maintained.

The differential settlements between the structure and the back-filling of the abutment deforms the geometry of the tracks. This causes the interaction forces between the train's wheels and the tracks to increase, which leads to an increase in the differential settlements. This mechanism repeats itself worsening the problem, until maintenance and repair are performed on the tracks [4]. This thesis neglects the interaction forces between the train's wheel and the tracks, and only focuses on the effects of stiffness variation in the system.

Several solutions have been applied to attempt solving this issue, like the implementation of "auxiliary rails" ([13], [18], [29]), under sleeper pads ([32], [25], [22], [14]), and even creating a gradual change of stiffness along the tracks ([32], [1], [17]). However, there is no evidence of this solutions working for extended periods of time (40 years or more), without requiring maintenance, or replacements of elements of the tracks.

This leads to the following research question:

What is the influence of introducing active control forces and moments in minimising the dynamic amplifications in railway transition zones?

The aim of this thesis is to study the effectiveness of implementing active control forces at the location of the interface of transition zone to diminish the dynamic amplification of the tracks.

1.3 Outline of the Thesis

This thesis contains 5 chapters. In Chapter 2 the research description is presented, along with previous studies on how to mitigate the deterioration of transition zones. Chapter 3 presents the description and derivation of the models, the derivation of the active control forces, as well as, a verification of Model A and Model B. Chapter 4 then presents a description of the findings and discussion of them. Then, Chapter 5, illustrates the conclusions and recommendations for further studies to be carried out in this topic.

Chapter 2

Literature Review and Research Methodology

2.1 Previous Studies

Throughout the years, several studies have been carried out to attempt attenuating the dynamic amplifications and differential settlements at transition zones. However, no definite solution has been found yet. In practice, there are several methods to reduce the degradation rate of transition zones, some of them are presented below.

Several researchers have studied the implementation of "auxiliary rails" in transition zones. This consists on adding extra rails to the sleepers over the transition zone, increasing the bending stiffness of the track. It helps for a better distribution of the loads on the sleepers. Consequently, this reduces the pressure acting on the ballast ([28], [11], [13], [18], [29]). However, in some cases, high stiffness also causes the dynamic forces in the wheel-rail interface, in the sleepers and in the ballast to increase, ultimately leading to wear and fatigue problems [12].

Another method that has been studied is the usage of "increasing sleepers' length" in the transition zone. This consists in gradually increasing the sleepers' length, width and height, while decreasing the spacing between them. This reduces the stresses and vertical displacements due to the increasing size of the area supporting the sleepers. ([28], [26]). However, this does not contribute much to the vertical stiffness as it also depends on the compaction and uniformity of the ballast ([21], [27], [3]).

Several authors suggest to create a smooth gradual change of stiffness along the tracks to minimize the increase of interaction forces at the transition zone ([32], [1], [17]). One method that has been widely studied is the implementation of "Under Sleeper Pads" between the ballast and the sleepers. This method consists in placing a rubber pad under the sleepers to reduce the sleeper-ballast interaction forces controlling the vertical stiffness of the tracks and increasing the track flexibility. This reduces the vibrations transmitted to the ballast by the passing train, as well as the resonance frequency of the system, however it increases receptance value of it ([32], [25], [2], [22], [14]).

Another aspect of the track system degradation is the localized settlements of the sleepers and the formation of voids under the sleepers, on which some may end up hanging. Extensive research

has been carried out on the dynamics behaviour of railway tracks with partially or fully unsupported sleepers ([34], [30], [33], [19], [15]). These studies showed that the presence of these hanging sleepers creates discontinuities and irregularities on the track support, which generates an increase on the wheel-rail interaction forces, further worsening the problem. This normally leads to worsen vehicle's stability and riding comfort. Paixao et al [24], studied the influence of back-fill settlements in the train-track interaction at transition zones. To do this, they performed non-linear dynamic analyses on a two dimensional model. They concluded that the back-fills with a wedge shape seem to limit the problems related to abrupt variations of the track's stiffness and differential settlements.

Another method that has been studied is the implementation of tuned mass dampers (TMD) in the system. This has been done mainly to suppress the noise radiation in the rails as in the work of Xiao et al [31]. However, Jouna [16], in his Master's thesis, studied the feasibility of placing distributed TMD along the tracks to lower the dynamic amplification provoked at the tracks due to the moving load in the transition zone. He concluded that the inclusion of these elements can lead to a significant reduction of the dynamic amplification of the system. However, it does not fully mitigate this response.

When looking at literature on numerical models, Faragau et al [10] formulated a model consisting of an Euler-Bernoulli beam resting on a inhomogeneous, non-linear Winkler foundation, subjected to a moving load. This research showed that the plastic deformation of the foundation is a consequence of constructive interference of the exited waves and the response of the system to the load's dead-weight. Then, Faragau et al [8], published a comparison of three solutions methods for one-dimensional models, the 'time-domain method', the 'integral-transform' method, and a hybrid method. They concluded that when dealing with non-linearities and inhomogeneities throughout the depth of the model, the 'time-domain' method is likely to be the most efficient method. Also, Faragau et al [9] studied the influence of accounting for the interaction between the vehicle and the supporting structure. For this, a one-dimensional model of an Euler-Bernoulli beam resting on a locally inhomogeneous Kelvin foundation was formulated. In terms of modelling of the foundation, Oliveira et al [5] derived a linear lattice model of the ballasts, to provide a framework to study the settlement of ballasts in zones of stiffness variation of the railway track support. Finally, Faragau [7], in his PhD dissertation, studied the initialization phase of differential settlements in transition zones, solely due to the amplification of stresses and strains occurring at these zones, due to a moving load. He demonstrated that the response amplification of the transition zone is due to the interference between the free field and the steady-state field of the system. The more pronounce the free field is, in comparison to the steady-state field, the more amplification is generated.

2.2 Research Description

This thesis will study the effectiveness of implementing active control forces and moments at the interface of transition zone to diminish the dynamic amplification of the tracks.

For this, two models of a transition zone were formulated from a starting point taken as a base model presented in [7]. The Base Model consists of an Euler-Bernoulli beam resting on a Winkler foundation. Then, the first model produced, takes a step further and connects the base of the Winkler foundation to a Shear beam which is also resting on step-wise inhomogeneous foundation, to achieve an Euler-Bernoulli beam resting on a Kerr foundation, this model is referred as Model A. Finally, the second model, which is referred to as 'Hybrid Model', represents the soft domain of the transition zone with the description of the first model, while the stiff domain of it is represented by the description of the Base Model. Moreover, all three models include active control forces and

moments in order to mitigate the dynamic amplification in the soft domain of the transition zone, on which the base model had to be adapted for this. Figure (2.1) illustrates the schematics of the three different models that are used in this thesis.

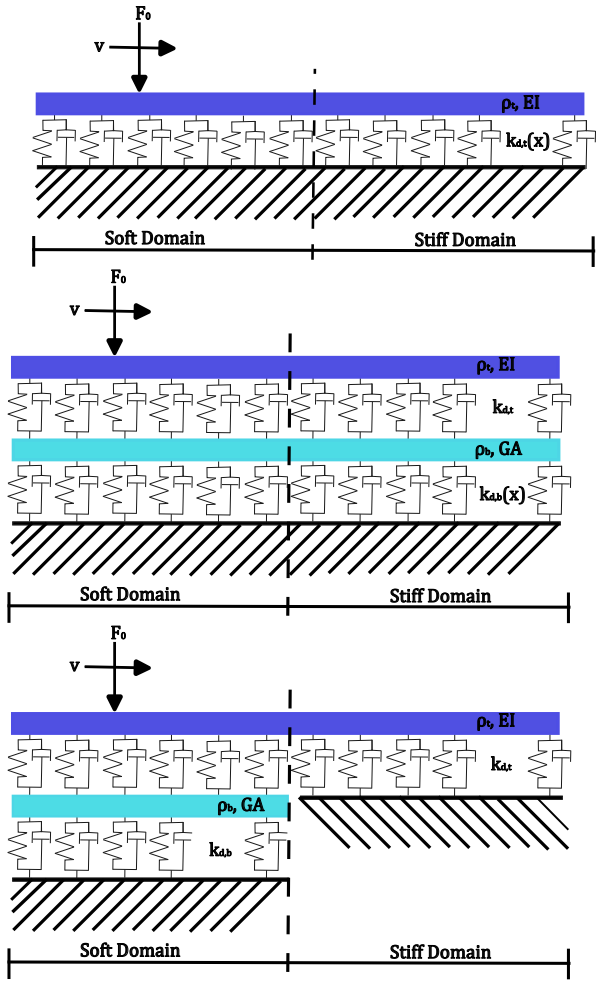

Figure 2.1: Schematics of the three models. Base Model (top panel), Kerr foundation (middle panel) and Hybrid Model (lower panel), where the vertical dashed line indicates a jump on stiffness at $x = x_{TC}$.

The reason of presenting three models is that the Base Model is a phenomenological model, which can approximate many scenarios of change in vertical stiffness. The second model, Model A, is formulated to better approximate the response of transition zones, as the lower (shear) beam incorporates effects of the foundation more precisely. Finally, the third model, the Hybrid Model, is formulated to represent a transition zone, on which the tracks go from earthworks, to a man-made structure; how could be the scenario of a concrete bridge or a culvert, on which the soil underneath the tracks is discontinued. Hence, the shear beam is not presented in the stiff zone of this model

because a rigid structure is considered under the first layer of springs and dash-pots (which represent the ballast). It must be noted that the second and third model are also phenomenological models.

Each of these models include active control forces and moments as a novel method to mitigate the dynamic amplifications in the soft domain of transition zones, when subjected to a constant moving load travelling from soft to stiff domains transition zones. The reason of including these active control forces and moments is that previous alternative solutions proposed by researchers do not fully achieve the desired mitigation in soft domains of transition zones.

Chapter 3

Models and Solutions

This section illustrates the derivation of the Base Model and the two extra models that were produced with the inclusion of the active control forces and moments. It also includes a overview on the derivation of the active control forces, on which the system of equations that must be solved for each model is presented. Moreover, a verification of the first and second model are presented along the error accumulated in their response. The Base Model, is presented here solely to show the adaptation of it. An extensive analysis have already been carried out by Andrei Faragau in [7]. Hence, the Base Model does not present any novelty and is not worth validating nor analysing in this thesis.

The Base Model, as it names may indicate, it is used as a base for the derivation of Model A and Model B (Hybrid Model). The first model, Model A, is an extension of the base one, on which a shear beam and a second layer of springs have been added, to achieve a Kerr foundation. These extra elements have been added to represent the mobilised soil under the tracks. The second model, Model B, is a hybrid model between the base one and the first one. This model seeks to better represent the transition zone by discontinuing the soil layer to better represent the interface interaction between the soft and rigid domains of transition zones.

3.1 Base Model - Euler-Bernoulli beam on a Winkler foundation

This section illustrates the derivation process of the active control force and moment required to be applied at the interface of the transition zone in order to completely mitigate the response amplification in the soft domain of the transition zone. The model consists on an Euler-Bernoulli beam resting on an piece-wise inhomogeneous Winkler foundation, the beam is subjected to a constant moving load, which also moves with constant velocity. To do this, first, the model is formulated with its corresponding interface and boundary conditions. Then, the steady-state solution of the system is obtained, as well as, the transient response of it. The system is analysed in the spatial frequency domain, by applying the Fourier transform over time. Finally, the active control force and moment, F_{EB} and M_{EB}, and the wave amplitudes of the system are derived. The time-domain counterparts are obtained by performing a numerical inverse Fourier transform.

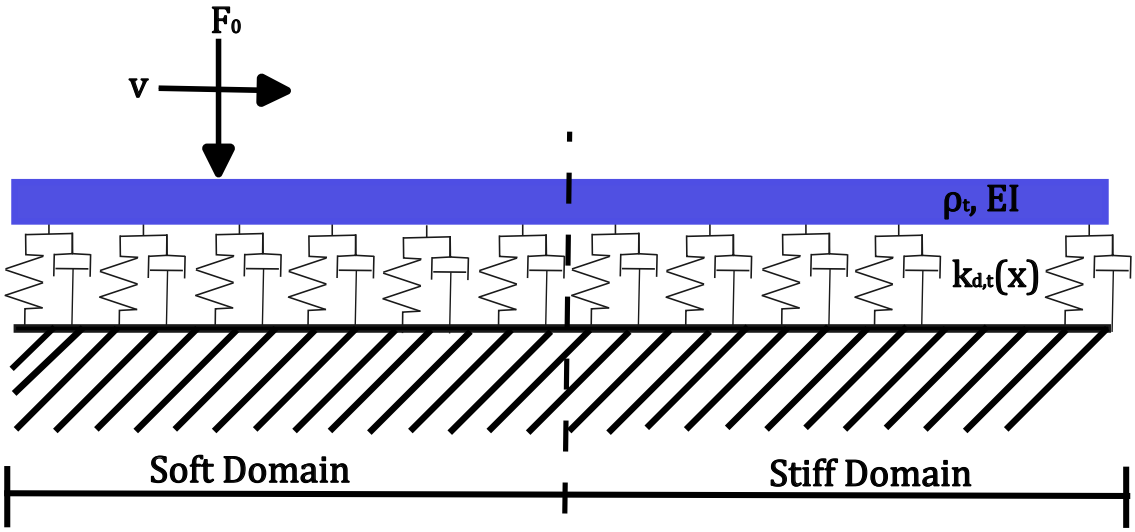

Figure 3.1: Model schematic: infinite Euler-Bernoulli beam on an inhomogeneous foundation, subjected to a constant moving load, where the vertical dashed line indicates a jump on stiffness at $x = X_{TC}$.

3.1.1 Model Formulation

The foundation of the model has a jump on stiffness at $x = x_{TC}$ (where the subscript stands for "Transition Centre"). This jump in stiffness divides the system in two semi-infinite domains. The equation of motion of the system is given below.

$$EI\frac{\partial^4 w(x,t)}{\partial x^4} + \rho\frac{\partial^2 w(x,t)}{\partial t^2} + k_d(x)w(x,t) = -F_0\delta(x - vt) \qquad w(x,t) = \begin{cases} w_L(x,t), & \text{for } x \leq x_{TC} \\ w_R(x,t), & \text{for } x \geq x_{TC} \end{cases}$$
$$k_d(x) = \begin{cases} k_{d,L}, & \text{for } x < x_{TC} \\ k_{d,R}, & \text{for } x \geq x_{TC} \end{cases} \tag{3.1}$$

Where $\frac{\partial}{\partial x}$ and $\frac{\partial}{\partial t}$ stands for the partial derivative with respect to space and time, respectively. EI is the bending stiffness of the beam and ρ is the mass per unit length of it. $k_{d,L}$ is the homogeneous foundation stiffness of the left semi-infinite domain, while $k_{d,R}$ is of the right semi-infinite domain. w_L and w_R represent the displacement field of the left and right semi-infinite domain, respectively. Furthermore, F_0 and v represent the magnitude and velocity of the constant moving load, respectively.

At the interface between the two domains, apart from imposing continuity in the displacement, slope, shear force balance and bending moment balance, an extra active control force and moment are imposed. These force and moment seek to ensure that no transient response is generated in the soft domain of the system (left domain) due to the moving load. Furthermore, the displacement at infinite distances from the moving load should not tend to infinity. Hence, the interface and boundary conditions read

$$w_L(x_{TC},t) = w_R(x_{TC},t) \tag{3.2}$$

$$w'_L(x_{TC},t) = w'_R(x_{TC},t) \tag{3.3}$$

$$w''_L(x_{TC},t) = w''_R(x_{TC},t) - \frac{M_{EB}(t)}{EI} \tag{3.4}$$

$$w'''_L(x_{TC},t) = w'''_R(x_{TC},t) - \frac{F_{EB}(t)}{EI} \tag{3.5}$$

$$\lim_{(x-vt)\to\infty} w_R(x,t) < \infty \tag{3.6}$$

$$\lim_{(x-vt)\to-\infty} w_L(x,t) < \infty \tag{3.7}$$

Where the primes denote classical partial derivatives with respect to x.

Moreover, as the system is infinite, and is only locally inhomogeneous, the response is assumed to be in the steady-state before the load reaches the transition zone. Hence, there is no need to formulate initial conditions. Therefore, Equations 3.1 to 3.7 constitute a complete description of the system. The next section derives the steady-state of the system.

3.1.2 Steady-State Solution

When $k_{d,L} = k_{d,R} = k_d$ the system described above becomes homogeneous, and consequently, its solution is in the steady-state for all time moments. The equation of motion of the system with an homogeneous Winkler foundation reads:

$$EI\frac{\partial^4 w(x,t)}{\partial x^4} + \rho\frac{\partial^2 w(x,t)}{\partial t^2} + k_d w(x,t) = -F_0\delta(x-vt) \tag{3.8}$$

To obtain the steady-state solution, the infinite domain is divided in two domains, in front of the moving load, w_f, and behind the moving load w_b. These domains are as follows:

$$w(x,t) = \begin{cases} w_b(x,t), & \text{for } x \le vt \\ w_f(x,t), & \text{for } x \ge vt \end{cases} \tag{3.9}$$

At the interface between both semi-infinite domains, continuity in displacement, slope, as well as shear forces and bending moments are imposed. Furthermore, the displacement at infinite distance from the moving load should not tend to infinity. Hence, the interface and boundary condition of the homogeneous solution of the system are:

$$w_b(vt,t) = w_f(vt,t) \tag{3.10}$$

$$w'_b(vt,t) = w'_f(vt,t) \tag{3.11}$$

$$w''_b(vt,t) = w''_f(vt,t) \tag{3.12}$$

$$w'''_b(vt,t) = w'''_f(vt,t) + \frac{F_0}{EI} \tag{3.13}$$

$$\lim_{x\to-\infty} w_b(x,t) < \infty \tag{3.14}$$

$$\lim_{x\to\infty} w_f(x,t) < \infty \tag{3.15}$$

The resulting equations of motion of both fields are now homogeneous. This is because the force has been transferred to the interface conditions expressing the vertical force equilibrium at $x = vt$.

The solution to the steady-state in the time-space domain can be assumed in the form of harmonic waves, as follows:

$$w_h(x,t) = A_h e^{i(\omega t - kx)}, \quad \text{for } h = [b, f] \tag{3.16}$$

Where subscripts "b" and "f" stand for behind and front, respectively, k denotes the wave number of the harmonic wave, and ω the frequency. Substituting the Homogeneous solution, eq. (3.16), into the equation of motion in the time domain, eq. (3.8), the dispersion equation is obtained, which reads:

$$\frac{EI}{\rho}(k^4 - \omega^2 + \omega_0^2) = 0 \tag{3.17}$$

Where ω_0 represents the cut-off frequency ($\omega_0 = \sqrt{\frac{k_d}{\rho}}$). To explicitly determine both ω and k, an additional equation is needed. This equation comes in the form of the kinematic invariant that relates the wavenumber, frequency and velocity of the moving load. The kinematic invariant is given by:

$$\omega = kv \tag{3.18}$$

When solving together the expression for the dispersion equation and the kinematic invariant, leads to four pairs $(\omega, k) = (\omega_{1-4}^e, k_{1-4}^e)$, which's natures depends upon the load velocity. Note that the subscript e is used to emphasise that these quantities are solutions of the dispersion equation and kinematic invariant, and are no longer variables.

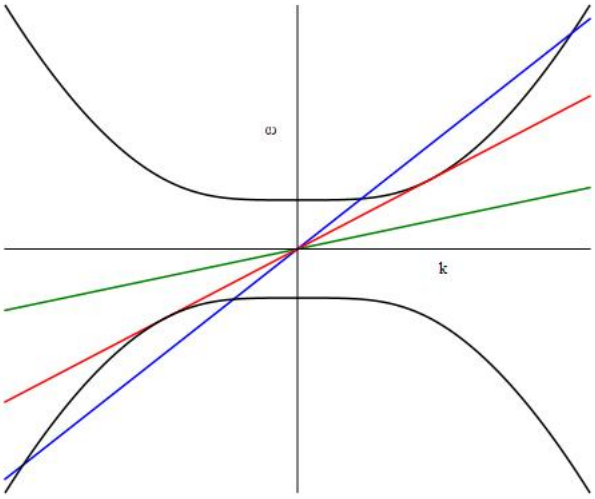

Figure 3.2: Dispersion curves Euler-Bernoulli beam on a Winkler foundation and kinematic invariant corresponding to three velocities: sub-critical (green), critical (red) and super-critical (blue).

The dispersion curves and the kinematic invariant are graphically represented in Figure (3.2). For velocities below the critical velocity (the velocity at which the system matches the cut-off frequency), there is no intersection between the kinematic invariant and the dispersion curves. This leads to complex-valued (ω^e, k^e) pairs. This means that the waves are evanescent for every (ω^e, k^e) pair, meaning that there is no energy radiating away from the load. For super-critical velocities, the kinematic invariant intersects the two dispersion curves at four locations. This gives real valued (ω^e, k^e) pairs. In this scenario, all waves and energy propagates away from the load. The last scenario is when the velocity of the system matches the critical velocity. This results in the kinematic invariant being tangential to the dispersion curves. This results in repeated real-valued (ω^e, k^e) pairs which induces resonance. The expression of the critical velocity of the system is:

$$c_{cr} = \sqrt[4]{\frac{4k_d EI}{\rho^2}} \tag{3.19}$$

With the known (ω^e, k^e) pairs, the solutions are given by:

$$w_h(x,t) = A_h e^{-ik_1^e(x-vt)} + b_h e^{-ik_2^e(x-vt)} + C_h e^{-ik_3^e(x-vt)} + D_h e^{-ik_4^e(x-vt)}, \quad \text{for } h = [b, f] \tag{3.20}$$

It must be noted that the above expression is not valid for when $v = c_{cr}$. Furthermore, the eight unknown amplitudes are determined from the interface and boundary conditions. Moreover, the wavenumbers of the eigenfield are chosen such that:

$$Re(k_1^e) > 0,\ Im(k_1^e) \geq 0, \tag{3.21}$$

$$Re(k_2^e) > 0,\ Im(k_2^e) \leq 0, \tag{3.22}$$

$$Re(k_3^e) < 0,\ Im(k_3^e) \leq 0, \tag{3.23}$$

$$Re(k_4^e) < 0,\ Im(k_4^e) \geq 0. \tag{3.24}$$

When applying the boundary conditions at infinite distances from the moving load, the wavenumbers k_2^e and k_3^e are admissible in the domain that extends to $-\infty$, and the k_1^e and k_4^e are admissible in the domain that extends to ∞. This leads to the $A_b = D_b = B_f = C_f = 0$. The eigenfield, in the time domain then becomes:

$$w^e(x,t) = \begin{cases} B_b e^{-ik_2^e(x-vt)} + C_b e^{-ik_3^e(x-vt)}, & \text{for } x < vt \\ A_f e^{-ik_1^e(x-vt)} + D_f e^{-ik_4^e(x-vt)}, & \text{for } x \geq vt \end{cases} \tag{3.25}$$

Hence, the eigenfield has been obtained in the time domain.

3.1.3 Transient Response

The response of the inhomogeneous system described in equations (3.1)-(3.7) is obtained applying the Fourier transform over time and the solution is represented by a summation of wave modes. The response obtained in the Fourier domain is analytical, while the inverse transform is performed numerically. The equation of motion in the Fourier domain reads

$$\frac{\partial^4 W(x,\omega)}{\partial x^4} + W(x,\omega)k^4(x) = -\frac{F_0}{EIv} e^{-i\omega\frac{x}{v}} \tag{3.26}$$

$$k(x,\omega) = \begin{cases} k_L = \sqrt[4]{-\frac{\rho}{EI}\omega^2 + \frac{k_{d,L}}{EI}}, & x < x_{TC} \\ k_R = \sqrt[4]{-\frac{\rho}{EI}\omega^2 + \frac{k_{d,R}}{EI}}, & x \geq x_{TC} \end{cases}$$

To determine the displacement field in the frequency domain, a particular solution is superimposed to the solution of the homogeneous equation. The particular solutions $W_{P,L}$ and $W_{P,R}$ are the frequency-domain eigenfield of the homogeneous system, with the properties of the left and right domain, respectively. These solutions were sought having the same spatial distribution as the forcing in the system and are given by the following equations:

$$W_{P,L}(x,\omega) = -\frac{F_0}{EI}\frac{v^3}{\omega^4 - k_L^4 v^4} e^{-i\omega\frac{x}{v}}, \quad \text{for } x \leq x_{TC} \tag{3.27}$$

$$W_{P,R}(x,\omega) = -\frac{F_0}{EI}\frac{v^3}{\omega^4 - k_R^4 v^4} e^{-i\omega\frac{x}{v}}, \quad \text{for } x > x_{TC} \tag{3.28}$$

The complete solutions to the displacement field in the frequency domain (including the solution of the homogeneous equation) is given as follows:

$$W_L(x,\omega) = A_L e^{-ik_L x} + B_L e^{ik_L x} + C_L e^{k_L x} + D_L e^{-k_L x} + W_{P,L}, \quad \text{for } x \leq x_{TC} \tag{3.29}$$

$$W_R(x,\omega) = A_R e^{-ik_R x} + B_R e^{ik_R x} + C_R e^{k_R x} + D_R e^{-k_R x} + W_{P,R}, \quad \text{for } x \geq x_{TC} \tag{3.30}$$

This thesis only focuses on sub-critical velocities. Hence, the four branches of the wave numbers, k_h (where $h = [L, R]$) are all complex values when ω is below the cut off frequency ($\omega_{co} = \sqrt{\frac{k_{d,h}}{\rho}}$). Throughout this thesis, the branches of k_h are chosen such that the imaginary part is negative and the real part is positive. This choice leads to ($A_L = D_L = B_R = C_R = 0$), when the boundary conditions, applied at infinite distance from the moving load, imposes a finite displacement. This leads to the following expression for the displacement field in the frequency domain:

$$W_L(x,\omega) = \begin{cases} B_L e^{ik_L x} + C_L e^{k_L x} + W_{P,L}, & \text{for } x \leq x_{TC} \\ A_R e^{-ik_R x} + D_R e^{-k_R x} + W_{P,R}, & \text{for } x \geq x_{TC} \end{cases} \tag{3.31}$$

The remaining four amplitudes are determined from interface conditions (Eqs. (3.2)-(3.5)) (note that to obtain the response of the unmodified transition zone, the forces F_{EB} and M_{EB} must be set to zero in the interface conditions). Then to obtain the solution in the time domain, the inverse Fourier transform was applied numerically.

3.1.4 Derivation of Active Forces and Moment

This sections derives the expressions of the active force and moment that can be applied at the interface of the transition zone, to ensure the mitigation of the transient response in the soft domain of the system (left domain). In order for this to happen, these forces must ensure that the magnitude of the amplitude of the free waves in the soft domain (B_L and C_L) are zero.

$$B_L = C_L = 0 \tag{3.32}$$

The forces are then obtained, in the frequency domain, by applying the interface conditions and solving for the two wave amplitude of the rigid domain, and for the active force and moment, F_{EB}

and M_{EB}, respectively. Then, an inverse Fourier transform is performed numerically in order to bring these force and moment, and the displacement field amplitudes into the time domain. The expressions are not given here due to brevity, however, they can be obtain straightforwardly by the use of a symbolic mathematical software (e.g. Maple).

3.2 Model A - Euler-Bernoulli Beam on an Inhomogeneous Kerr Foundation

The model formulated in this section, an Euler-Bernoulli on an inhomogeneous Kerr foundation (also known as a two-parameter elastic foundation), is superior than the one in the previous section, a Euler-Bernoulli beam on a Winkler foundation. This is because of the inclusion of the shear beam and the bottom layer of springs. These elements have been added to represent the mobilised soil under the tracks. This way, a better understanding on the stresses arising at the different parts of the system can be achieved, namely the stresses at the track level, and at the soil under the tracks. For this, a similar derivation as the previous section to derived the active forces is performed. First, the model is formulated with its corresponding interface and boundary conditions. Then, the steady-state solution of the system is obtained, as well as, the transient response of it. The system is analysed in the spatial frequency domain, by applying the Fourier transform over time. Finally, the active forces and moment, F_{EB}, F_S and M_{EB}, and the wave amplitudes of the system are derived. The time-domain counterparts are obtained by performing a numerical inverse Fourier transform.

3.2.1 Model Formulation

The model of the transition zone formulated in this section is a two-layer model. It consists of an infinite Euler-Bernoulli beam with bending stiffness EI, and linear density ρ_t and a shear beam, with shear stiffness GA and linear density ρ_b. Both beams are connected by a layer of springs with stiffness $k_{d,t}$. The shear beam rests on a Winkler foundation of stiffness $k_{d,b}$ (the subscripts "t" and "b" stand for top and bottom, respectively, referring to either the top or the bottom layer of springs). Similarly as in Chapter 2, there is a jump of stiffness at $x = x_{TC}$, in this case, only in the bottom layers of springs. The system is shown in Figure (3.1) and its equations of motion are:

$$EI\frac{\partial^4 w(x,t)}{\partial x^4} + \rho_t \frac{\partial^2 w(x,t)}{\partial t^2} + k_{d,t}(w(x,t) - u(x,t)) = -F_0\delta(x - vt) \tag{3.33}$$

$$-GA\frac{\partial^2 u(x,t)}{\partial x^2} + \rho_b \frac{\partial^2 u(x,t)}{\partial t^2} + u(x,t)(k_{d,t} + k_{d,b}(x)) - w(x,t)k_{d,t} = 0 \tag{3.34}$$

$$w(x,t) = \begin{cases} w_L(x,t) & x \leq x_{TC} \\ w_R(x,t) & x \geq x_{TC} \end{cases} \qquad k_{d,b}(x) = \begin{cases} k_{d,b,L} & x < x_{TC} \\ k_{d,b,R} & x \geq x_{TC} \end{cases}$$

$$u(x,t) = \begin{cases} u_L(x,t) & x \leq x_{TC} \\ u_R(x,t) & x \geq x_{TC} \end{cases}$$

Where w and u are the displacement fields of the Euler-Bernoulli beam and of the shear beam, respectively.

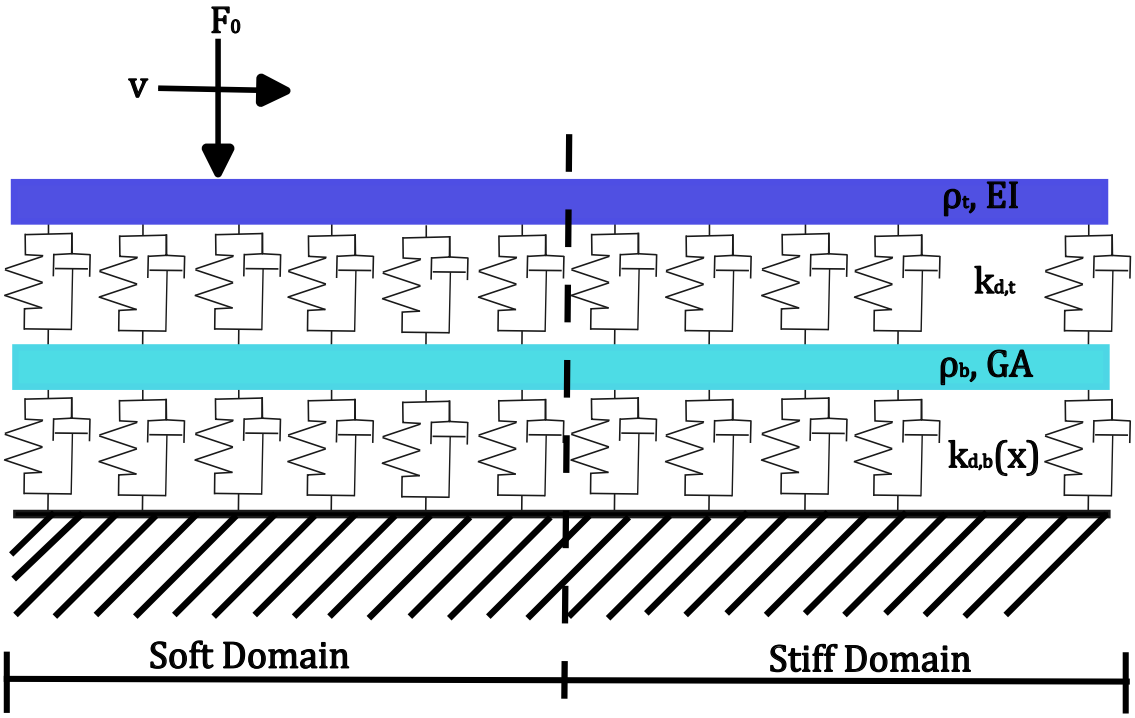

Figure 3.3: Model schematic: infinite Euler-Bernoulli beam on a Kerr foundation, where the vertical dashed line indicates a jump on stiffness in the bottom layer of springs at $x = x_{TC}$.

At the interface between the two domains ($x = x_{TC}$), the same conditions as in Section 3.1 are applied to the Euler-Bernoulli beam. Namely, continuity in displacement and slope, as well as in shear force and bending moment, with the inclusion of an extra force and moment at the interface of the transition zone (Eqs. (3.2)-(3.5)). Similarly as in Section 3.1, these forces seek to mitigate the transient response in the soft domain of the system (left domain). Moreover, the conditions applied at infinite distance from the moving load are also the same as in Section 3.1 (Eqs. (3.6) and (3.7)). For the shear beam, two interface conditions are required, these conditions ensure the continuity of displacement and shear forces in the beam. This model also includes an extra force at the interface centre, which also seeks to mitigate the transient response of the system in the soft domain of the system. Moreover, the displacement of the shear beam at infinite distance from the moving load should not tend to infinity. Hence, the added interface and boundary conditions due to the inclusion of a shear beam are:

$$u_L(x_{TC}, t) = u_R(x_{TC}, t) \tag{3.35}$$

$$u'_L(x_{TC}, t) = u'_R(x_{TC}, t) + \frac{F_S(x)}{GA} \tag{3.36}$$

$$\lim_{x\to\infty} u_R(x, t) < \infty \tag{3.37}$$

$$\lim_{x\to-\infty} u_L(x, t) < \infty \tag{3.38}$$

Similarly to the situation in Section 3.1, the initial conditions do not influence the response in the vicinity of the transition zone, hence, there is no need to formulate initial conditions. Therefore, Eqs. (3.33)-(3.38) together with Eqs. (3.2)-(3.7) constitute a complete description of the problem. The next section derives the steady-state of the system.

3.2.2 Steady-State Solution

When both layers of springs have constant stiffness throughout the infinite domain, the system becomes homogeneous, and consequently, its response to the moving load is in the steady-state. The characteristics of the steady-state solution, as seen in Section 3.1, helps in understanding the transient response. Consequently, the steady-state response is derived first. To obtain the solution in this scenario, we use the same approach described in Section 3.1.2, which is to divide the infinite domain in two semi-infinite ones, namely behind and in front of the moving load.

$$EI\frac{\partial^4 w(x,t)}{\partial x^4} + \rho_t \frac{\partial^2 w(x,t)}{\partial t^2} + k_{d,t}(w(x,t) - u(x,t)) = -F_0\delta(x - vt) \tag{3.39}$$

$$-GA\frac{\partial^2 u(x,t)}{\partial x^2} + \rho_b \frac{\partial^2 u(x,t)}{\partial t^2} + u(x,t)(k_{d,t} + k_{d,b}) - w(x,t)k_{d,t} = 0 \tag{3.40}$$

$$w(x,t) = \begin{cases} w_b(x,t) & x \leq x_{TC} \\ w_f(x,t) & x \geq x_{TC} \end{cases}$$

$$u(x,t) = \begin{cases} u_b(x,t) & x \leq x_{TC} \\ u_f(x,t) & x \geq x_{TC} \end{cases}$$

At the interface between both semi-infinite domains, continuity in displacement, slope, as well as, shear forces and moments are imposed. Furthermore, the displacements at infinite distance from the moving load should not tent to infinity. Hence, the interface and boundary conditions that must be added to those presented in Section 3.1.2 (eqs. (3.10)-(3.15)) are:

$$u_b(vt,t) = u_f(vt,t) \tag{3.41}$$

$$u_b'(vt,t) = u_f'(vt,t) \tag{3.42}$$

$$\lim_{x\to-\infty} u_b(x,t) < \infty \tag{3.43}$$

$$\lim_{x\to\infty} u_f(x,t) < \infty \tag{3.44}$$

The resulting equations of motion, of both fields, now are homogeneous. This is because the force of the moving load has been transferred to the interface conditions expressing the vertical force equilibrium at $x = vt$.

Moreover, similarly as in Section 2.2, the solution of the homogeneous equations of motion can be assumed in the form of harmonic waves, as follows:

$$W_h(x,t) = A_h e^{i(\omega t - kx)}, \quad \text{for } h = [b,f] \tag{3.45}$$

$$U_h(x,t) = B_h e^{i(\omega t - kx)}, \quad \text{for } h = [b,f] \tag{3.46}$$

After substituting the assumed solutions in the equations of motion, in order to obtain non-trivial solutions, the determinant of the system is set to zero, resulting in the dispersion equation of the system:

$$ak^6 + bk^4 + ck^2 = 0 \tag{3.47}$$

where
$a = EIGA$
$b = EI(-\omega^2\rho_b + k_{d,b} + k_{d,t})$
$c = GA(-\omega^2\rho_t + k_{d,t})$
$d = \omega^4\rho_b\rho_t - \omega^2 k_{d,b}\rho_t - k_{d,t}\omega^2(\rho_b + \rho_t) + k_{d,b}k_{d,t}$

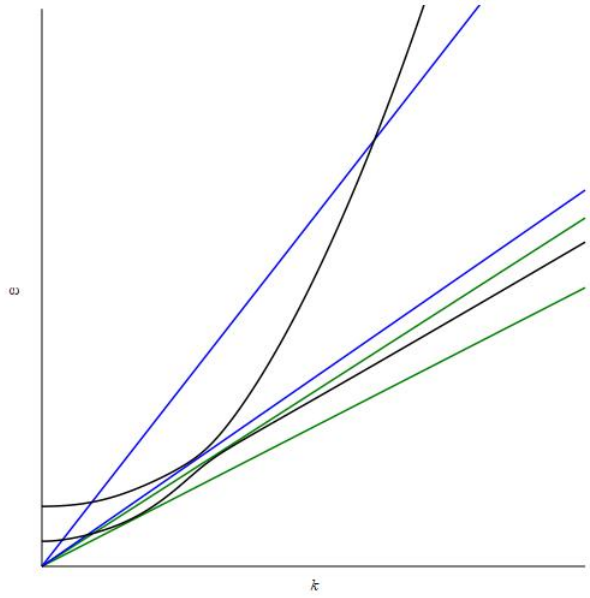

Figure 3.4: Dispersion curves Euler-Bernoulli beam on a Kerr foundation

It can be seen that the dispersion equation is a polynomial of order six in k. This means that compared to the system in Section 3.1 (which has a polynomial of order four, see Eq. (3.17)), the system with an additional shear beam, has two additional solutions for the wave-number, meaning that its solution is composed of six waves instead of four. Similarly to the system in Section 3.1, the nature of the waves in the system with an additional shear beam depends upon the velocity of the moving load. Moreover, the waves' nature also depend upon the shear stiffness and linear weight of the shear beam. To determine the types of waves, we first need to solve the system of equations consisting of the dispersion equation and the kinematic invariant for k. The dispersion curve is graphically presented in Fig. (3.4). The two-layer system has four dispersion curves (two for positive frequencies and two for negative ones). The additional curves appear because the dispersion equation has a term proportional to ω^4, while in the previous case the highest power of ω, in the dispersion equation, was two.

From the dispersion curves from Fig. (4.2) it can be seen that the system posses 3 critical velocities (the velocities at which the kinematic invariant is tangential to one of dispersion curves, and at which the system undergoes resonance-like behaviour). The first lowest critical velocity is given when the kinematic invariant is tangential to lower part of the lower branch dispersion curve. This sets the change in the behaviour of the system, going from having only evanescent waves to have at least one pair of propagating waves. The next critical velocity is given when the kinematic invariant is tangential to the upper part of the lower dispersion curve branch. When the velocity of the moving load is between the first and the second critical velocity, the kinematic invariant intersects the dispersion curve at three distinct points, meaning that the solution is composed of three pairs of propagating waves. The final critical velocity is given when the kinematic invariant is tangential to the upper dispersion curve branch. When the velocity of the system is between the second and the third critical velocity, the kinematic invariant intersects the dispersion curve only at one point, meaning that the solution is composed of 1 pair of propagating waves, and 2 pairs of evanescent waves. Finally, when the velocity of the moving load is greater than the third critical velocity, the solution of the system is composed of 3 pairs of propagating waves, as the kinematic invariant intersects the lower dispersion curve branch at one location and the upper at two distinct locations. For this system, sub-critical regime is considered when the velocity of the moving load is less than the first critical velocity of the system. This implies that for any sub-critical velocities, the system will not have any propagating waves.

With the known pairs (ω^e,k^e), the solutions in the time domain are given by the following expressions:

$$\begin{aligned} W_h(x,t) = A_{1h}e^{-ik_1^e(x-vt)} + A_{2h}e^{-ik_2^e(x-vt)} + A_{3h}e^{-ik_3^e(x-vt)} + A_{4h}e^{-ik_4^e(x-vt)} \\ +A_{5h}e^{-ik_5^e(x-vt)} + A_{6h}e^{-ik_6^e(x-vt)}, \quad \text{for } h=[b,f] \\ U_h(x,t) = B_{1h}e^{-ik_1^e(x-vt)} + B_{2h}e^{-ik_2^e(x-vt)} + B_{3h}e^{-ik_3^e(x-vt)} + B_{4h}e^{-ik_4^e(x-vt)} \\ +B_{5h}e^{-ik_5^e(x-vt)} + B_{6h}e^{-ik_6^e(x-vt)}, \quad \text{for } h=[b,f] \end{aligned} \tag{3.48}$$

The twelve unknown amplitudes are determined from the interface and boundary conditions. Since the system now has 6 new complex-valued wavenumbers, the choice of wavenumbers of the eigenfield given in Eqs.(3.21)-(3.24) have to be adapted. To do this, two more conditions are imposed, which are:

$$Re(k_5^e) > 0, \quad Im(k_5^e) < 0, \tag{3.49}$$

$$Re(k_6^e) < 0, \quad Im(k_6^e) > 0, \tag{3.50}$$

Throughout this thesis, the branches of k_h are chosen such that the imaginary part of the wavenumbers is negative and the real part positive. This choice leads to $A_{4b} = A_{5b} = A_{6b} = A_{1f} = A_{2f} = A_{3f} = 0$ when the boundary conditions, applied at infinite distance from the moving load, imposes a finite displacement. This is the shape of the solution for the parameters that we use (that lead to the dispersion curves presented above) and for sub-critical velocities. For other parameter choices and for the super-critical velocities, the shape of the solution can be different with 4 waves behind the load and only 2 in front. The eigenfield, in the time domain, then becomes:

$$W^e(x,t) = \begin{cases} A_{1b}e^{-ik_1^e(x-vt)} + A_{2b}e^{-ik_2^e(x-vt)} + A_{3b}e^{-ik_3^e(x-vt)}, & \text{for } x < vt \\ A_{4f}e^{-ik_4^e(x-vt)} + A_{5f}e^{-ik_5^e(x-vt)} + A_{6f}e^{-ik_6^e(x-vt)}, & \text{for } x \geq vt \end{cases} \tag{3.51}$$

$$U^e(x,t) = \begin{cases} B_{1b}e^{-ik_1^e(x-vt)} + B_{2b}e^{-ik_2^e(x-vt)} + B_{3b}e^{-ik_3^e(x-vt)}, & \text{for } x < vt \\ B_{4f}e^{-ik_4^e(x-vt)} + B_{5f}e^{-ik_5^e(x-vt)} + B_{6f}e^{-ik_6^e(x-vt)}, & \text{for } x \geq vt \end{cases} \tag{3.52}$$

It must be noted that the amplitudes A and B are related through the eigenvectors as follows: $B_n = A_n q^e_{n,2}$, where $n = [1, ..., 6]$ and $q^e_{n,2}$ represents the second entry in the corresponding nth eigenvector, as shown in eq. (3.53) as follows:

$$B_n = -\frac{EIk_n^4 - \rho_t\omega^2 + k_{d,t}}{k_{d,t}} A_n \tag{3.53}$$

Then the eigenfield in the time domain has been obtained.

3.2.3 Transient Response

Similarly to Section 3.1.3, to obtain the response of the inhomogeneous system, the Fourier transform was applied, and the solutions to the displacement fields are sought in the form of a summation of wave modes. The equation of motion representing the inhomogeneous system in the Fourier domain reads:

$$EI\frac{\partial^4 W(x,\omega)}{\partial x^4} + W(x,\omega)(-\rho_t\omega^2 + k_{d,t}) + U(x,\omega)k_{d,t} = -\frac{F}{v}e^{-i\omega\frac{x}{v}} \tag{3.54}$$

$$-GA\frac{\partial^2 U(x,\omega)}{\partial x^2} + U(x,\omega)(-\rho_b\omega^2 + k_{d,b}(x) + k_{d,t}) - W(x,\omega)k_{d,t} = 0 \tag{3.55}$$

To determine the displacement fields in the frequency domain, particular solutions are imposed to the solutions of the homogeneous equation (for the Euler-Bernoulli and the shear beam). The particular solutions W_P and U_P are the frequency-domain eigenfield of the homogeneous system, with the properties of the left and right domain, depending upon the location with respect to the interface of the transition cnetre. These solutions were sought having the same spatial distribution as the forcing in the system and are given by the following equation:

$$W_{P,h}(x,\omega) = \frac{Fv^3(a_h\omega^2 + v^2(EI(k_{d,b,h} + k_{d,t})))}{EI(a_h\omega^6 + v^2(b_h\omega^4 + v^2(c_h\omega^2 + v^2d_h)))}e^{-i\omega\frac{x}{v}} \tag{3.56}$$

$$U_{P,h}(x,\omega) = \frac{Fv^5k_{d,t}}{EI(a_h\omega^6 + v^2(b_h\omega^4 + v^2(c_h\omega^2 + v^2d_h)))}e^{-i\omega\frac{x}{v}} \tag{3.57}$$

$$\begin{aligned} a_h &= EI(-\rho_b v^2 + GA) \\ b_h &= v^4\rho_b\rho_t - v^2GA\rho_t + EI(k_{d,b,h} + k_{d,t}) \\ c_h &= -(((\rho_b - \rho_t)k_{d_t} + k_{d,b,h}\rho_t)v^2 - GAk_{d,t}) \\ d_h &= k_{d,b,h}k_{d,t} \end{aligned} \qquad h = \begin{cases} L, & x < x_{TC} \\ R, & x \geq x_{TC} \end{cases}$$

The solution in the Fourier domain (after applying the boundary conditions at infinity), reads:

$$W(x,\omega) = \begin{cases} A_{L1}e^{-ik_1x} + A_{L2}e^{-ik_2x} + A_{L3}e^{-ik_3x} + W_{P,L}, & \text{for } x \leq x_{TC} \\ A_{R4}e^{-ik_4x} + A_{R5}e^{-ik_5x} + A_{R6}e^{-ik_6x} + W_{P,R}, & \text{for } x \geq x_{TC} \end{cases} \tag{3.58}$$

$$U(x,\omega) = \begin{cases} B_{L1}e^{-ik_1 x} + B_{L2}e^{-ik_2 x} + B_{L3}e^{-ik_3 x} + U_{P,L}, & \text{for } x \leq x_{TC} \\ B_{R4}e^{-ik_4 x} + B_{R5}e^{-ik_5 x} + B_{R6}e^{-ik_6 x} + U_{P,R}, & \text{for } x \geq x_{TC} \end{cases} \tag{3.59}$$

Where the wave amplitudes of the top and bottom domain are related by the expression given in Eq. (3.53).

The unknown amplitudes can be obtained from the interface conditions (Eqs. (3.2)-(3.7) and (3.35)-(3.38)) (note that to obtain the response of the unmodified transition zone, the forces F_{EB}, F_S and M_{EB} must be set to zero in the interface conditions). Then the solutions in the time domain are obtained by numerically evaluating the inverse Fourier transform over the displacement field in the frequency domain.

3.2.4 Derivation of Active Forces and Moment

This sections derives the expressions of the active forces and moments that can be applied at the interface of the transition zone, to ensure the mitigation of the transient response in the soft domain of the system (left domain). In order for this to happen, these forces and moment must ensure that the magnitude of the amplitude of the waves in the soft domain (A_{L1},A_{L2} and A_{L3}) are zero.

$$A_{L1} = A_{L2} = A_{L3} = 0 \tag{3.60}$$

Replacing the above conditions, into the expressions for the complete solution to the displacement field, given in Section 3.2.3, in Eqs. (3.58) and (3.59), we obtained the expression for the complete solution to the displacement field of the adapted transition zone as follows:

$$W(x,\omega) = \begin{cases} W_{P,L}, & \text{for } x \leq x_{TC} \\ A_{R4}e^{-ik_4 x} + A_{R5}e^{-ik_5 x} + A_{R6}e^{-ik_6 x} + W_{P,R}, & \text{for } x > x_{TC} \end{cases} \tag{3.61}$$

$$U(x,\omega) = \begin{cases} U_{P,L}, & \text{for } x \leq x_{TC} \\ B_{R4}e^{-ik_4 x} + B_{R5}e^{-ik_5 x} + B_{R6}e^{-ik_6 x} + U_{P,R}, & \text{for } x > x_{TC} \end{cases} \tag{3.62}$$

Now the interface conditions (Eqs. (3.2)-(3.5) and (3.35)-(3.36)) can be applied in the above equations, which yields the following system of equations:

$$\begin{bmatrix} -e^{ik_{R4}x_{TC}} & -e^{k_{R5}x_{TC}} & -e^{k_{R6}x_{TC}} & 0 & 0 & 0 \\ -ik_{R4}e^{ik_{R4}x_{TC}} & -ik_{R5}e^{k_{R5}x_{TC}} & -ik_{R6}e^{k_{R6}x_{TC}} & 0 & 0 & 0 \\ k_{R4}^2 e^{ik_{R4}x_{TC}} & k_{R5}^2 e^{k_{R5}x_{TC}} & k_{R6}^2 e^{k_{R6}x_{TC}} & \frac{1}{EI} & 0 & 0 \\ ik_{R4}^3 e^{ik_{R4}x_{TC}} & ik_{R5}^3 e^{k_{R5}x_{TC}} & ik_{R6}^3 e^{k_{R6}x_{TC}} & 0 & \frac{1}{EI} & 0 \\ -B_{R4}e^{ik_{R4}x_{TC}} & -B_{R5}e^{k_{R5}x_{TC}} & -B_{R6}e^{k_{R6}x_{TC}} & 0 & 0 & 0 \\ -iB_{R4}e^{ik_{R4}x_{TC}} & -iB_{R5}e^{k_{R5}x_{TC}} & -iB_{R6}e^{k_{R6}x_{TC}} & 0 & 0 & -\frac{1}{GA} \end{bmatrix} \begin{pmatrix} A_{R4} \\ A_{R5} \\ A_{R6} \\ M_{EB} \\ F_{EB} \\ F_S \end{pmatrix} =$$

$$= \begin{pmatrix} W_{P,R} - W_{P,L} \\ (W_{P,R} - W_{P,L})(-i\omega/v) \\ (W_{P,R} - W_{P,L})(-i\omega/v)^2 \\ (W_{P,R} - W_{P,L})(-i\omega/v)^3 \\ U_{P,R} - U_{P,L} \\ (U_{P,R} - U_{P,L})(-i\omega/v) \end{pmatrix}$$

The system of equations was then solved numerically, in the frequency domain, solving for the three wave amplitude of the rigid domain (A_{R4}, A_{R5}, A_{R6}), and for the active forces and moment

(F_{EB}, F_S and M_{EB}). Then, an inverse Fourier transform was performed numerically in order to bring the interface forces and the displacement field amplitudes into the time domain. It is important to note that this system of equations cannot be solved analytically due to its complexity.

To verify that the correct active forces and moment are obtained, a small verification is carried out. For this, the interface conditions (Eqs. (3.2)-(3.5) and (3.35)-(3.36)) are replaced in the complete solution of the displacement field given in Section 3.2.3, in Eqs. (3.58) and (3.59), which yields the following system of equations:

$$\begin{bmatrix} e^{ik_{L1}x_{TC}} & e^{ik_{L2}x_{TC}} & e^{ik_{L3}x_{TC}} & -e^{ik_{R4}x_{TC}} & -e^{k_{R5}x_{TC}} & -e^{k_{R6}x_{TC}} \\ ik_{L1}e^{ik_{L1}x_{TC}} & ik_{L2}e^{ik_{L2}x_{TC}} & ik_{L3}e^{ik_{L3}x_{TC}} & -ik_{R4}e^{ik_{R4}x_{TC}} & -ik_{R5}e^{k_{R5}x_{TC}} & -ik_{R6}e^{k_{R6}x_{TC}} \\ -k_{L1}^2e^{ik_{L1}x_{TC}} & -k_{L2}^2e^{ik_{L2}x_{TC}} & -k_{L3}^2e^{ik_{L3}x_{TC}} & k_{R4}^2e^{ik_{R4}x_{TC}} & k_{R5}^2e^{k_{R5}x_{TC}} & k_{R6}^2e^{k_{R6}x_{TC}} \\ -ik_{L1}^3e^{ik_{L1}x_{TC}} & -ik_{L2}^3e^{ik_{L2}x_{TC}} & -ik_{L3}^3e^{ik_{L3}x_{TC}} & ik_{R4}^3e^{ik_{R4}x_{TC}} & ik_{R5}^3e^{k_{R5}x_{TC}} & ik_{R6}^3e^{k_{R6}x_{TC}} \\ B_{L1}e^{ik_{L1}x_{TC}} & B_{L2}e^{ik_{L2}x_{TC}} & B_{L3}e^{ik_{L3}x_{TC}} & -B_{R4}e^{ik_{R4}x_{TC}} & -B_{R5}e^{k_{R5}x_{TC}} & -B_{R6}e^{k_{R6}x_{TC}} \\ iB_{L1}e^{ik_{L1}x_{TC}} & iB_{L2}e^{ik_{L2}x_{TC}} & iB_{L3}e^{ik_{L3}x_{TC}} & -iB_{R4}e^{ik_{R4}x_{TC}} & -iB_{R5}e^{k_{R5}x_{TC}} & -iB_{R6}e^{k_{R6}x_{TC}} \end{bmatrix}$$

$$\begin{pmatrix} A_{L1} \\ A_{L2} \\ A_{L3} \\ A_{R4} \\ A_{R5} \\ A_{R6} \end{pmatrix} = \begin{pmatrix} W_{P,R} - W_{P,L} \\ (W_{P,R} - W_{P,L})(-i\omega/v) \\ (W_{P,R} - W_{P,L})(-i\omega/v)^2 - \frac{F_{EB}}{EI} \\ (W_{P,R} - W_{P,L})(-i\omega/v)^3 - \frac{M_{EB}}{EI} \\ U_{P,R} - U_{P,L} \\ (U_{P,R} - U_{P,L})(-i\omega/v) + \frac{F_S}{GA} \end{pmatrix}$$

Then, the system of equation is solved to obtain the wave amplitudes of the soft domain, when the magnitude of the active forces is set to 0, to obtain the wave amplitudes of a transition zone without the inclusion of these forces. Then the system is solved by including the magnitude of the active forces that were obtained previously. To bring the wave amplitudes to the time domain, and inverse Fourier transform was performed numerically.

Figure (3.5) illustrates a comparison between the absolute value of the wave amplitudes of a normal transition zone and a transition zone that includes the active forces and moment, in the frequency domain. It can be seen that these forces completely mitigate the amplitudes of the waves in the soft domain of the transition zone. Hence, the correct active forces and moment are obtained.

3.2.5 Work Done by the Active Control Forces and Moments

To calculate the work done by the active control forces and moment, the spectral energy density was calculated, and then integrated over the frequency domain. For this, the following equations illustrates how to calculate this:

$$E_{F_{EB}} = -\frac{1}{2\pi}\int_{-\infty}^{\infty}(i\omega F_{EB}(\omega)(w(x = x_{TC}, \omega)))d\omega \tag{3.63}$$

$$E_{M_{EB}} = -\frac{1}{2\pi}\int_{-\infty}^{\infty}(i\omega M_{EB}(\omega)(w'(x = x_{TC}, \omega)))d\omega \tag{3.64}$$

$$E_{F_S} = -\frac{1}{2\pi}\int_{-\infty}^{\infty}(i\omega F_S(\omega)(u(x = x_{TC}, \omega)))d\omega \tag{3.65}$$

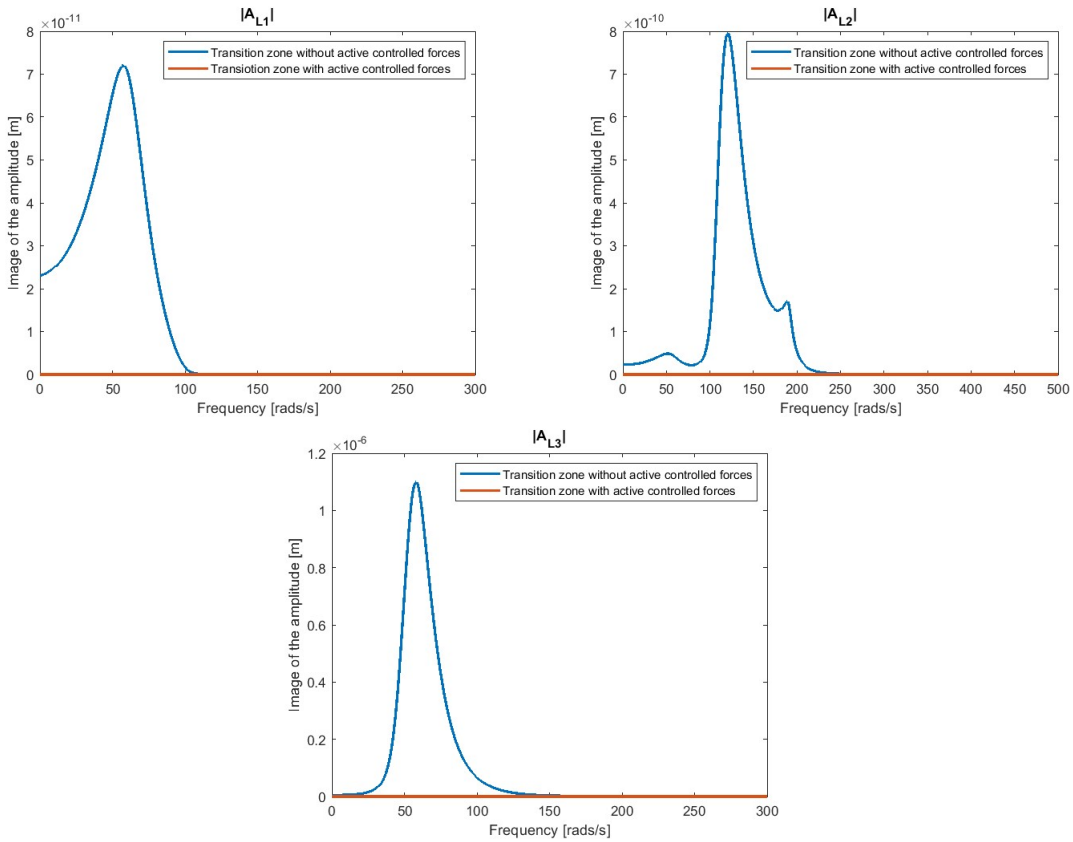

Figure 3.5: Comparison between the amplitudes of the absolute value of the image of the waves in the soft domain for a transition zone with and without the active forces and moment, in the frequency domain.

3.2.6 Verification Model A

To validate the model, a limit case is considered, in which the foundation is piece-wise homogeneous. To do this, the bottom layer of springs is set to be homogeneous and infinitely stiff; i.e. $k_{d,b,L} = k_{d,b,R} = 6.86 * 10^{290} N/m$. The shear beam was also set to be infinitely stiff; i.e. $GA = 2.68 * 10^{290} N/m^2$, while the coefficient of stiffness of the stiff domain of top layer of spring, $k_{d,t,R}$, is set equal to $k_{d,t,L}$.

The limit case solution is compared to the analytical steady-state solution of the Base Model, derived in Section (3.1.3). The error, $E(x)$, which is presented in Figure (3.6) is defined as the summation over time of the absolute value of the difference between the limit case solution of Model A, w_{ModelA} and the benchmark solution, which is given by the Base Model, $w_{BaseModel}$, divided by the summation of the benchmark solution over time, as follows:

$$E(x) = \frac{\sum_{t=0}^{tmax} |w_{ModelA}(x,t) - w_{BaseModel}(x,t)|}{\sum_{t=0}^{tmax} |w_{BaseModel}(x,t)|} \tag{3.66}$$

It can be seen that some error is accumulated in the solution of Model A, however it is of very small magnitude.

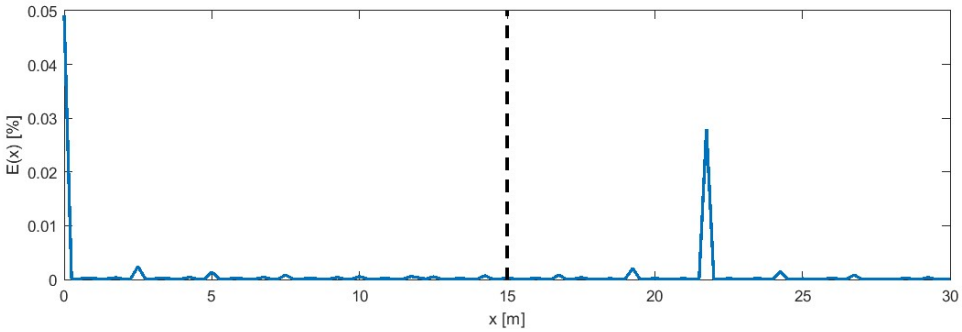

Figure 3.6: Error accumulated versus space, as defined in Eq. (3.66), for the limit case considered in Model A.

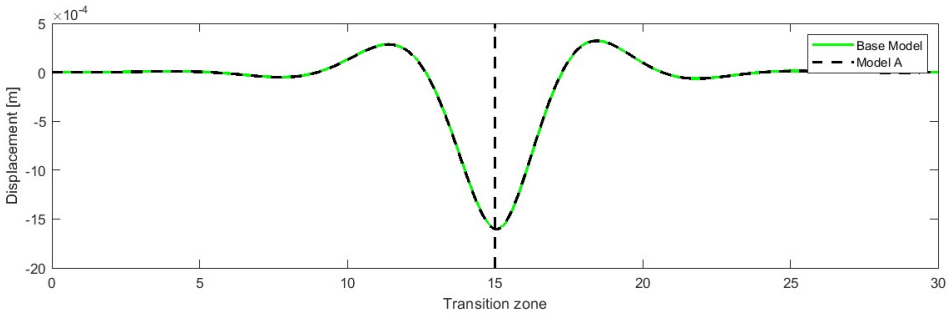

Figure 3.7: Comparison of the response of Model A, subjected to the limit case, and the Base Model.

Figure (3.7) illustrates a snapshot of the response of Model A under the limit case, when the moving load is at the interface of the transition zone. This figure also includes the behaviour of the Base Model. Both models are subjected to 75% of the critical velocity of the systems. It can be concluded, that there is a very good correlation between the behaviour of the Base Model and Model A when subjected to the limit case. Therefore, it can be assumed that the model produced is accurate and trustworthy.

For the verification of the model, the relevant parameters summarised in Table 3.1, were used. For the Base Model, the parameters of the Euler-Bernoulli beam, and the top spring layers were adopted.

3.3 Model B - Hybrid Model

The model formulated in this section represents the soft domain of the transition zone as an Euler-Bernoulli beam resting on a double parameter foundation (Model A), while the stiff zone of the

Amplitude of the load exerted by the train F	$20,000N$
Mass per unit length of the tracks, ρ_t	$974.165kg/m$
Bending stiffness of the tracks, EI	$6.42 * 10^6 Nm^2$
Distributed spring stiffness of the top spring layer, $k_{d,t}$	$6.7 * 10^6 N/m$
Top spring layer damping	$8,078.9Ns/m^2$
Shear stiffness of the shear beam, GA	$2.68 * 10^7 N/m^2$
Mass per unit length of the shear beam, ρ_b	$2020kg/m$
Distributed spring stiffness of the bottom spring layer (soft domain), $k_{d,b}$	$6.86 * 10^6 N/m$
Bottom spring layer damping	$77,693Ns/m^2$

Table 3.1: Parameters used for modelling of the transition zone.

transition zone is represented by a Euler Bernoulli beam on a Winkler foundation (Base Model). The Euler-Bernoulli beam is subjected to a constant amplitude moving load, which moves with constant velocity. This model is a different scenario of a transition zone, on which there is a discontinuity of the shear beam into the rigid domain.

To do this, the same steps are followed as in Section 3.2, and are repeated here for the reader's convenience. First, the model is formulated with its corresponding interface and boundary conditions. Then, the steady-state solution of the system is obtained, as well as, the transient response of it. The system is analysed in the spatial frequency domain, by applying the Fourier transform over time. Finally, the active control forces and moment, F_{EB}, F_S and M_{EB}, and the wave amplitudes of the system are derived, and brought back to the time domain by performing a numerical inverse Fourier transform.

3.3.1 Model Formulation

The model of the transition zone is a hybrid between the model presented in Section 3.1, and the model presented in Section 3.2. It's soft domain is represented by the model in Section 3.2, a continuous Euler-Bernoulli and a shear beam. Both beams are connected by means of a homogeneous layer of springs, with stiffness $k_{d,t}$. The shear beam is also resting on a Winkler foundation of stiffness $k_{d,b}$ (note that the subscript t and b stand for top and bottom, respectively). The rigid domain of the transition zone is represented by the model formulated in Section 3.1, a continuous Euler-Bernoulli beam, which rests on a Winkler foundation with the same properties as the top layer of springs of the soft domain. Similarly as in the previous models, the transition zone is located at $x = x_{TC}$. Which in this model represent the location at which the shear beam and the bottom layer of springs are discontinued. In this model the end of the shear beam is considered as a free-end. The system is shown in Figure (3.8) and its equations of motion are:

For $x \leq x_{TC}$:

$$EI\frac{\partial^4 w(x,t)}{\partial x^4} + \rho_t \frac{\partial^2 w(x,t)}{\partial t^2} + k_{d,t}(w(x,t) - u(x,t)) = -F_0\delta(x - vt) \tag{3.67}$$

$$-GA\frac{\partial^2 u(x,t)}{\partial x^2} + \rho_b \frac{\partial^2 u(x,t)}{\partial t^2} + u(x,t)(k_{d,t} + k_{d,b}) - w(x,t)k_{d,t} = 0 \tag{3.68}$$

For $x > x_{TC}$:

$$EI\frac{\partial^4 w(x,t)}{\partial x^4} + \rho_t \frac{\partial^2 w(x,t)}{\partial t^2} + k_{d,t}(w(x,t)) = -F_0\delta(x - vt) \tag{3.69}$$

$$w(x,t) = \begin{cases} w_L(x,t), & \text{for } x \leq x_{TC} \\ w_R(x,t), & \text{for } x \geq x_{TC} \end{cases}$$

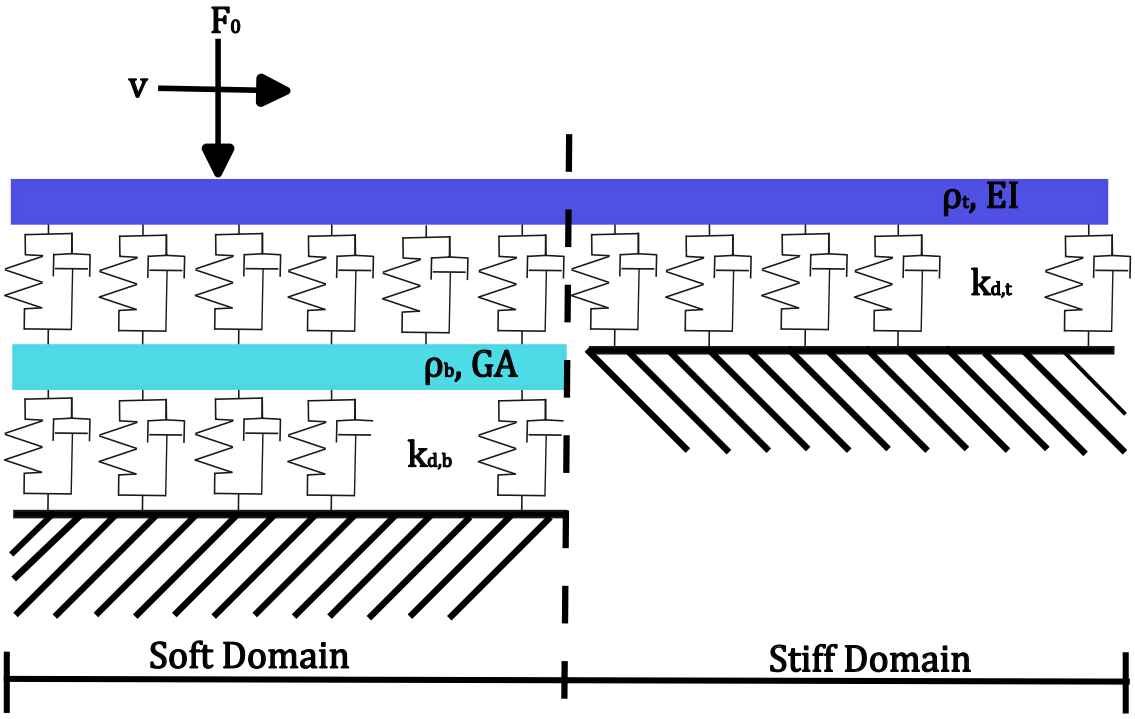

Figure 3.8: Model schematic: Hybrid Model, where the vertical dashed line represents a jump of stiffness, at $x = x_{TC}$.

At the interface between the two domains ($x = x_{TC}$), the same conditions as in Section 3.1 are applied to the Euler-Bernoulli beam. Namely, continuity in displacement and slope, as well as in shear force balance and bending moment balance, with the inclusion of an extra force and moment at the interface of the transition zone (Eqs. (3.2)-(3.5)). Similarly as in Section 3.1.1, these forces seek to mitigate the dynamic amplification in the soft domain of the system (left domain). Moreover, the conditions applied at infinite distance from the moving load are also the same as in Section 3.1.1 (Eqs. (3.6) and (3.7)). For the shear beam, two boundary conditions are required. At $x = x_{TC}$, the end of the shear beam is free, hence the shear force is equal to the active control force, and in its absence, the boundary condition describes a free end. Moreover, the displacement of the shear beam at infinite distance from the moving load should not tend to infinity, which is

described by eq. (3.38) in Section 3.2.1. Hence, the new boundary conditions of a shear beam are at the location of the transition zone is:

$$u'_L(x_{TC}, t) = -\frac{F_S(t)}{GA} \tag{3.70}$$

Where the primes denote classical partial derivatives with respect to x.

Similarly to the previous models in Section 3.1.1 and Section 3.2.1, the initial conditions do not influence the response in the vicinity of the transition zone, hence, there is no need to formulate initial conditions. Therefore, Eqs. (3.67)-(3.69) together with Eqs. (3.2)-(3.7), (3.37) and Eq. (3.70) constitute a complete description of the problem. Moreover, when the load is far away from the transition zone to its left, the steady-state is described by Eq. (3.25) and to its right by Eqs. (3.51) and (3.52).

3.3.2 Transient Response

Similarly as in the previous sections, to obtain the response of the inhomogeneous system, the Fourier transform was applied, and the solutions to the displacement field were sought in the form of a summation of wave modes. The equations of motion representing the inhomogeneous system in the Fourier domain reads:

For $x \leq x_{TC}$:

$$EI\frac{\partial^4 W(x,\omega)}{\partial x^4} + W(x,\omega)(-\rho_t\omega^2 + k_{d,t}) + U(x,\omega)k_{d,t} = -\frac{F_0}{v}e^{-i\omega\frac{x}{v}} \tag{3.71}$$

$$-GA\frac{\partial^2 U(x,\omega)}{\partial x^2} + U(x,\omega)(-\rho_b\omega^2 + k_{d,b} + k_{d,t}) - W(x,\omega)k_{d,t} = 0 \tag{3.72}$$

For $x \geq x_{TC}$:

$$EI\frac{\partial^4 W(x,\omega)}{\partial x^4} + W(x,\omega)(-\rho_t\omega^2 + k_d) = -\frac{F_0}{v}e^{-i\omega\frac{x}{v}} \tag{3.73}$$

To determine the displacement fields in the frequency domain, particular solutions are imposed to the solutions of the homogeneous solutions (for the Euler-Bernoulli beam and the shear beam). The particular solution of Euler-Bernoulli beam and shear beam's displacement field of the left domain of the system is given by eq. (3.56) and eq. (3.57), respectively. On other hand, the particular solution that must be imposed on the right domain of the system is given by eq. (3.28).

The solution in the Fourier domain (after applying the boundary conditions at infinity), reads:

$$W(x,\omega) = \begin{cases} A_{L1}e^{-ik_1x} + A_{L2}e^{-ik_2x} + A_{L3}e^{-ik_3x} + W_{P,L}, & \text{for } x \leq x_{TC} \\ A_{R3}e^{-ik_3x} + A_{R4}e^{-ik_4x} + W_{P,R}, & \text{for } x \geq x_{TC} \end{cases} \tag{3.74}$$

$$U(x,\omega) = \left\{ B_{L1}e^{-ik_1x} + B_{L2}e^{-ik_2x} + B_{L3}e^{-ik_3x} + U_{P,L}, \quad \text{for } x \leq x_{TC} \right. \tag{3.75}$$

Where the wave amplitudes of the top and bottom domain are related by the expression given in Eq. (3.53).

The unknown amplitudes can be obtained from the interface conditions (Eqs. (3.2)-(3.5), (3.35) and (3.70)) (note that to obtain the response of the unmodified transition zone, the forces F_{EB}, F_S and M_{EB} must be set to zero in the interface conditions). Then the solutions in the time domain are obtained by numerically evaluating the inverse Fourier transform over the displacement field in the frequency domain.

3.3.3 Derivation of Active Control Forces and Moments

This section derives the active control forces and moments that can be applied at the interface of the transition zone, such that the transient response in the soft domain of the system (left domain) is mitigated. For this to happen, these forces must ensure that the magnitude of the amplitude of the waves in the soft (A_{L1},A_{L2} and A_{L3}) domain are zero.

$$A_{L1} = A_{L2} = A_{L3} = 0 \tag{3.76}$$

Replacing the above conditions, into the expressions for the complete solution to the displacement field, given in Section 3.3.2, in Eqs. (3.74) and (3.59), we obtained the expression for the complete solution to the displacement field of the adapted transition zone as follows:

$$W(x,\omega) = \begin{cases} W_{P,L}, & \text{for } x \leq x_{TC} \\ A_{R3}e^{-ik_3 x} + A_{R4}e^{-ik_4 x} + W_{P,R}, & \text{for } x \geq x_{TC} \end{cases} \tag{3.77}$$

$$U(x,\omega) = U_{P,L}, \text{ for } x \leq x_{TC} \tag{3.78}$$

Now the interface conditions (eqs. (3.2)-(3.5) and (3.70)) can be applied in the above equations, which yields the following system of equations:

$$\begin{bmatrix} -e^{-ik_R x_{TC}} & -e^{-k_R x_{TC}} & 0 & 0 & 0 \\ ik_R e^{-ik_R x_{TC}} & k_R e^{-k_R x_{TC}} & 0 & 0 & 0 \\ k_R^2 e^{-ik_R x_{TC}} & -k_R^2 e^{-k_R x_{TC}} & \frac{1}{EI} & 0 & 0 \\ -ik_R^3 e^{-ik_R x_{TC}} & k_R^3 e^{-k_R x_{TC}} & 0 & \frac{1}{EI} & 0 \\ 0 & 0 & 0 & 0 & -\frac{1}{GA} \end{bmatrix} \begin{pmatrix} A_{R3} \\ A_{R4} \\ M_{EB} \\ F_{EB} \\ F_S \end{pmatrix} = \begin{pmatrix} W_{P,R} - W_{P,L} \\ (W_{P,R} - W_{P,L})(-i\omega/v) \\ (W_{P,R} - W_{P,L})(-i\omega/v)^2 \\ (W_{P,R} - W_{P,L})(-i\omega/v)^3 \\ -U_{P,L}(-i\omega/v) \end{pmatrix}$$

The system of equations was then solved numerically, in the frequency domain, solving for the three wave amplitude of the rigid domain (A_{R4}, A_{R5}, A_{R6}), and for the interface forces (F_{EB}, F_S and M_{EB}). Then, an inverse Fourier transform was performed numerically in order to bring the interface forces and the displacement field amplitudes into the time domain.

The verification of the derivation of the correct active fores and moment was done as for the previous model in Section 3.2.4, but was not presented here to avoid repetition.

3.3.4 Verification Model B

To validate the solution of the Hybrid Model, a limit case is considered, in which the foundation is piece-wise homogeneous. To do this, the bottom layer of springs is set to be infinitely stiff; i.e. $k_{d,b} = 6.86 * 10^{290} N/m$, as well as, the shear beam; i.e. $GA = 2.68 * 10^{290} N/m^2$, while the coefficient of stiffness of the stiff domain of the top layer of springs stiffness, $k_{d,t,R}$, is set equal to the one in the soft domain, $k_{k,t,L}$.

The limit case is compared to the analytical steady-state solution of the Base Model, derived in Section (3.1.3). The error, $E(x)$, which is presented in Figure (3.9) is defined as the summation over time of the absolute value of the difference between the limit case solution of the Hybrid Model, $w_{HybridModel}$ and the benchmark solution, which is given by the Base Model, $w_{BaseModel}$, divided by the summation of the benchmark solution over time, as follows:

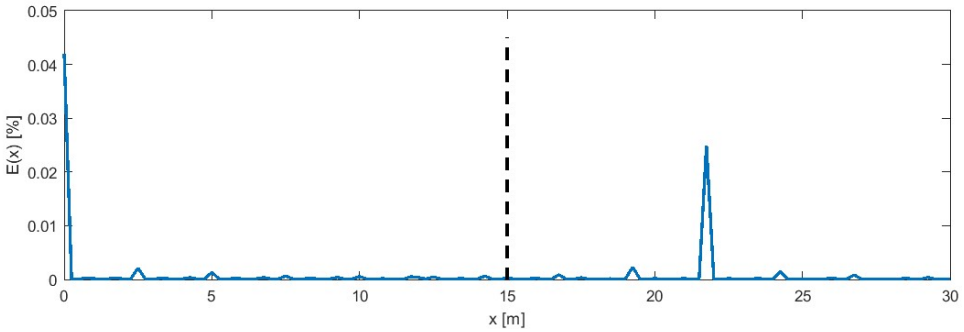

Figure 3.9: Error accumulated versus space, as defined in Eq. (3.79), for the limit case considered in the Hybrid Model.

$$E(x) = \frac{\sum_{t=0}^{tmax} |w_{HybridModel}(x,t) - w_{BaseModel}(x,t)|}{\sum_{t=0}^{tmax} |w_{BaseModel}(x,t)|} \tag{3.79}$$

It can be seen that some error is accumulated in the solution of the Hybrid Model, however it is of very small magnitude.

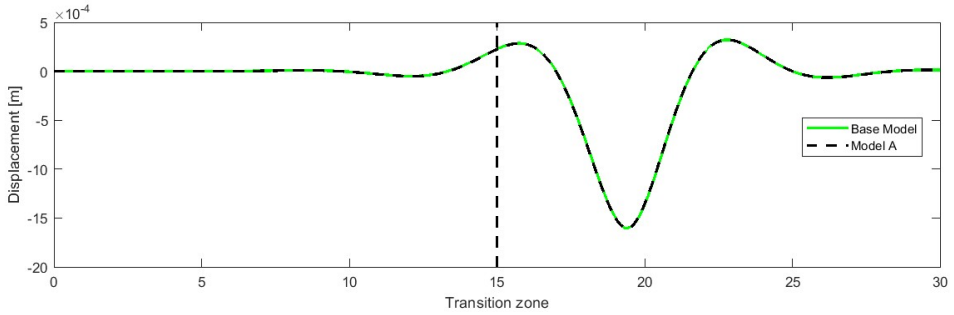

Figure 3.10: Comparison of the response of the Hybrid Model, subjected to the limit case, and the Base Model.

Figure (3.10) illustrates a snapshot of the response of the Hybrid Model when the moving load is at the interface of the transition zone. This figure also includes the behaviour of the Base Mode. This figure also includes the behaviour of the Base Model. Both models are subjected to 75% of the critical velocity of the systems. It can be concluded, that there is a very good correlation between the behaviour of the Base Model and the Hybrid Model when subjected to the limit case. Therefore, it can be assumed that the model produced is accurate and trustworthy.

For the verification of this model, the parameters shown in Table 3.1 were used.

Chapter 4

Findings and discussion

This section presents and analyzes the outcomes of deriving the active control forces and moments crucial for mitigating the transient response of the soft domain within the developed transition zone models. It comprises three subsections: the first two showcase results from Model A (Euler-Bernoulli beam on a Kerr foundation) and Model B (hybrid model), respectively, while the third subsection offers a comparative discussion of the findings obtained from both models.

4.1 Results Model A

First, the behaviour of the transition zone without the inclusion of the interface forces is studied. To do this, the displacement close to the transition zone is analysed, and compared to the displacement under the load for when the moving load is sufficiently far away (in the soft domain) of the transition zone, to not get affect by it. The left panel of Figure (4.1) represents the displacement under the load far away of the transition zone, for different velocities of the moving load. As it can be seen in the displacement plot far away from the transition zone, the critical velocity of the system is given at the point on which the response reaches an extreme value, which marks the transition from sub-critical to super-critical regime (when the relative velocity equals 1), the second critical velocity occurs when the relative velocity of the system 1.19, and the third critical velocity at 1.31. The displacement under the load increases with increasing velocities of the moving load for sub-critical velocities, while it decreases with increases velocities for super-critical regime. The right panel of Figure (4.1) illustrates the maximum displacement under the moving load for when the load is close to the transition zone, for various foundation stiffness ratios. The stiffness ratio, $P = \frac{k_{d,b,L}}{k_{d,b,R}}$, is defined as the relationship between the soft to stiff stiffness of the bottom layer of springs of the model. It can be seen that the system amplifies its response with increasing velocity of the moving load, reaching a maximum at critical velocity, once this velocity is passed, the response of the system decreases. Moreover, it can also be observed that the amplification of the response close to the transition zone also increases with increasing stiffness ratio.

Figure (4.2) illustrates the force amplification of the transition zone along the tracks, for a system with and without the inclusion of the active control forces, when subjected to a constant moving load of 75% of the critical velocity of the system, and a stiffness ratio, P, equal to 2. It can be seen that the force amplification in the soft domain (to the left of the vertical dashed line) has been completely mitigated in both beams, when the system has active control forces, meaning that

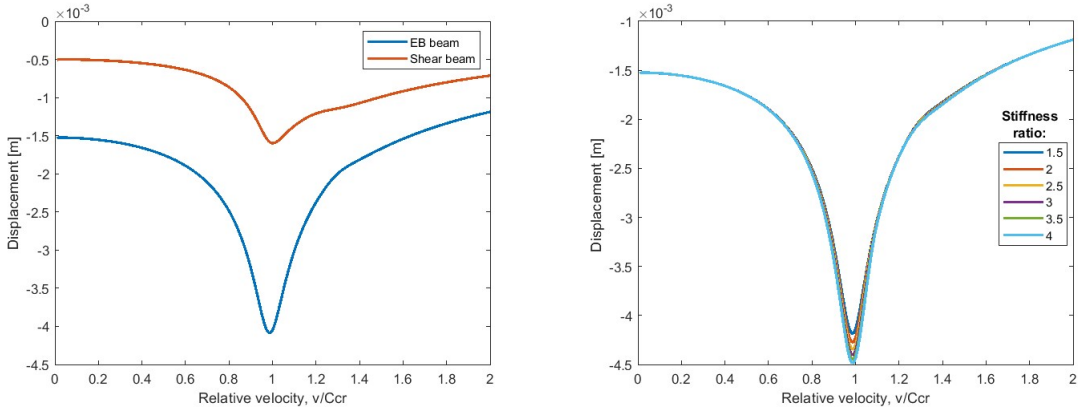

Figure 4.1: Maximum displacement under the moving load; far from the transition zone (left panel), and close to the transition zone (right panel) of Model A.

it responds in its steady-state until the moving load reaches the interface. However, when looking at the stiff domain (to the right of the vertical dashed line), it can be seen that the forces in the component of the system amplify, leading to higher displacements under the moving load in the beams. It can also be seen that this force amplification extends to $10m$ in the proximity of the transition zone.

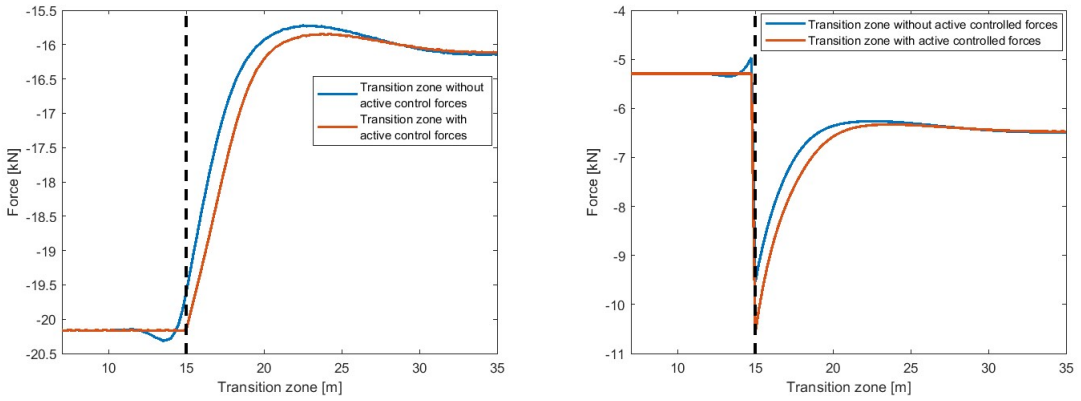

Figure 4.2: Maximum force experienced at both springs levels in Model A over time. Top spring layer (left panel) and bottom spring layer (right panel).

The time history comparison of the behavior of the active control forces and moment are presented in Figure (4.3), for several velocities, and a stiffness ratio, P, equal to 2. The duration of the active control forces and moment over time can be seen to decrease with increasing velocity of the moving load. Moreover, apart from reducing on their reaction time, the active forces and moment, as the velocity of the moving load approaches the critical velocity, starts developing opposite sign peaks much smaller in amplitude than the main peak. The higher the velocity of the moving load

(once the wavy pattern starts), the more 'wavy' the active forces and moment become over time.

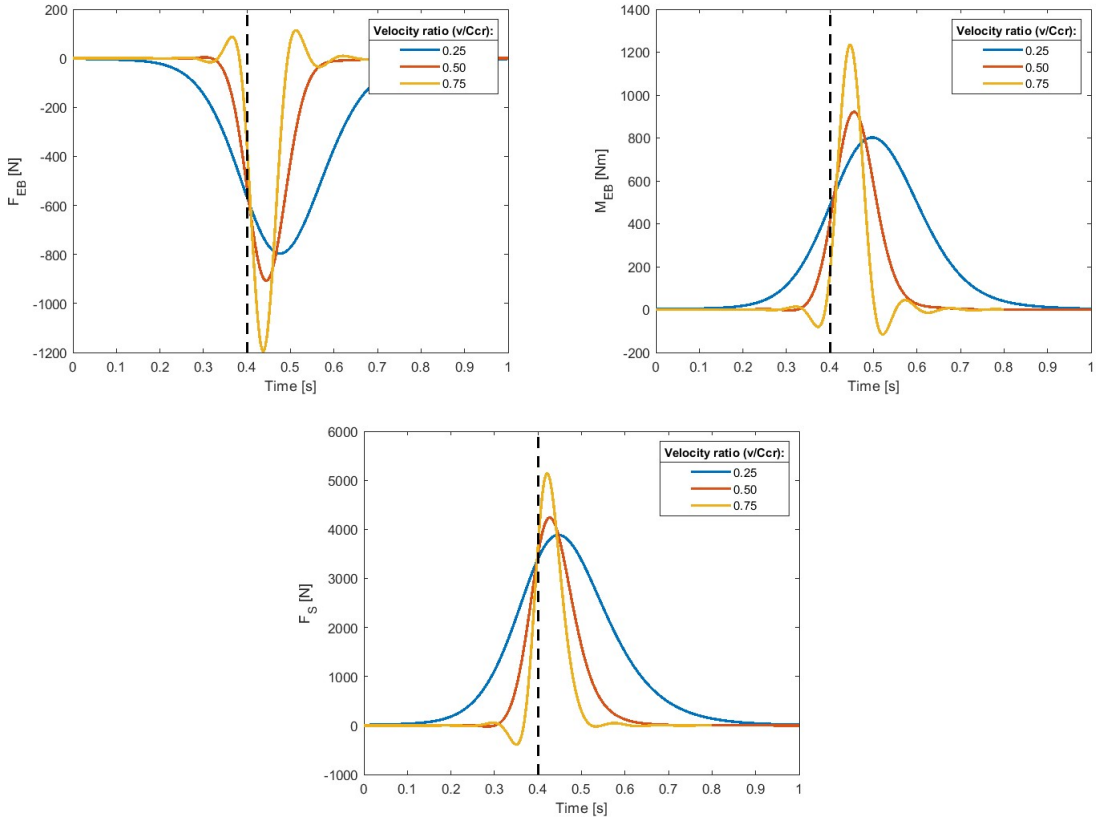

Figure 4.3: Time history comparison of the behaviour of the active control forces and moment of Model A, for a stiffness ratio equal to 2, for several specific velocities. The dashed line indicates the moment in time when the moving load crossed over the interface of the transition zone.

Figure (4.4) depicts the energy required by the active control forces and moment to mitigate the transient response in the soft domain of the transition zone for various velocities. It can be seen that the active control force acting at the Euler-Bernoulli beam and at the shear beam are responsible of absorbing energy out of the system, while the active moment acting at the Euler-Bernoulli beam adds energy into the system. It can be seen that the peak in absorption and addition of energy in the system happens at critical velocity, regardless of the stiffness ratio of the system. Moreover, the higher the stiffness ratio, the more energy that is absorbed and added into the system by the active control forces and moment. It can be noted that for low stiffness ratio (e.g. 1.5 or smaller), the active contorl force acting on the Euler-Bernoulli beam tends to input some energy into the system, but it mostly absorbs energy out of the system, while for higher stiffness ratios, this active control force only absorbs energy.

The impact of stiffness ratio on the response of the interface forces also deserves scrutiny. Figure (4.5) illustrates this analysis. The figure illustrates the energy required by the interface forces to

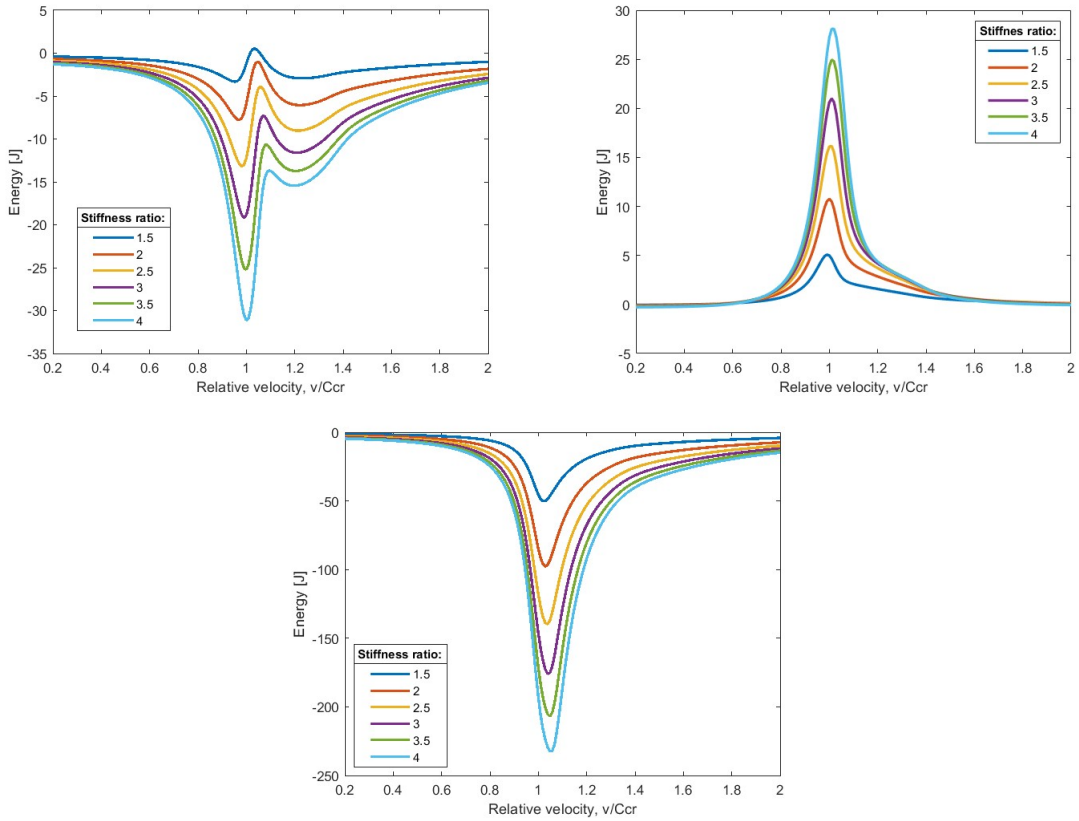

Figure 4.4: Energy required by the active control forces and moment applied at the interface of the transition zone of Model A in order to mitigate the transient response, for varying velocities, while keeping constant several stiffness ratios. Shear force at Euler-Bernoulli beam (top-left panel), Moment at Euler-Bernoulli beam (top-right panel), and shear force at shear beam (bottom panel)

mitigate the transient response in the soft domain of the system for various stiffness ratios, while keeping the velocity of the moving load constant. It can be seen that for relatively low velocities (less than 50% of the critical velocity of the system), the difference in energy requirements by the active control forces and moments are negligible, while for higher velocities, there is a large difference in the energy required, which increases with increasing stiffness ratios. It can also be seen that at critical velocities the energy requirements of the active control forces and moments is at its maximum.

Investigating the extreme values of forces and moments in response to varying stiffness ratios and velocities also yields insightful findings. Figure (4.6) illustrates these extreme values for different stiffness ratios as the velocity changes. It can be seen that as the stiffness ratio of the transition zone increases, the peaks of these forces tend to shift further into the super-critical regime. Moreover, the response of the moment imposed at the Euler-Bernoulli beam demonstrates solely positive amplitudes when the velocity is below 50% of the critical velocity. Conversely, for the same ve-

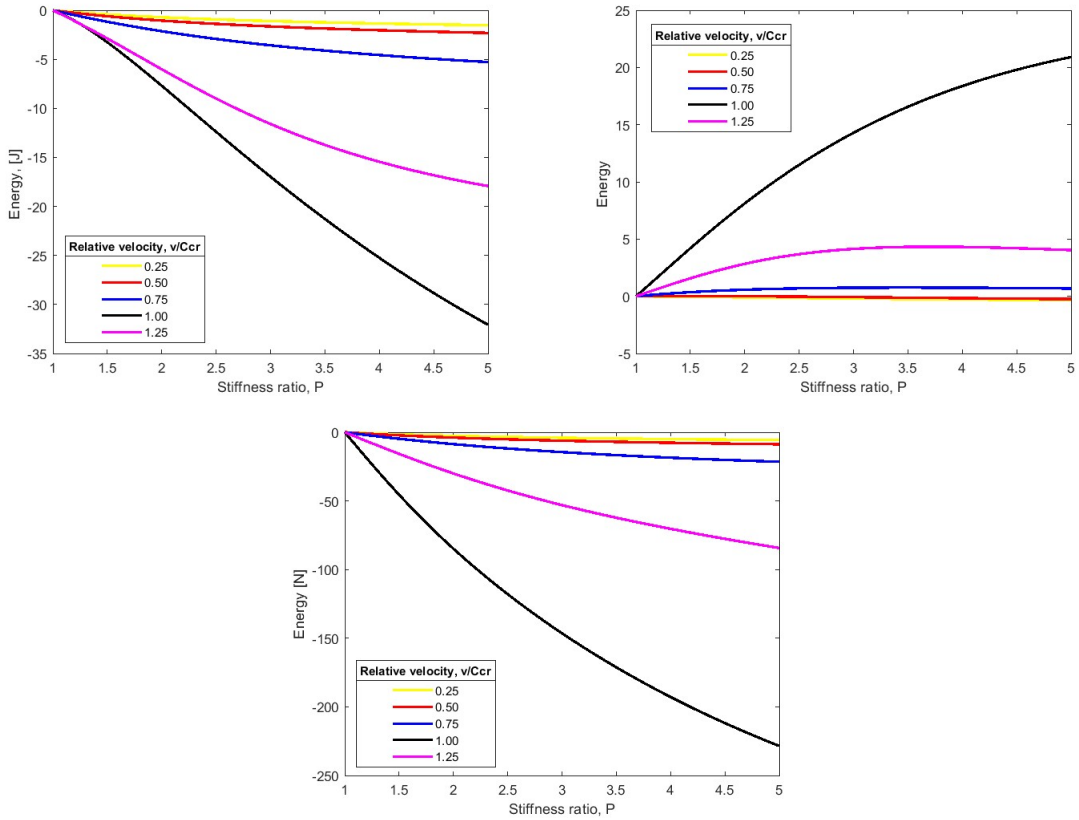

Figure 4.5: Energy required by the active control forces and moment applied at the interface of the transition zone of Model A in order to mitigate the transient response, for varying stiffness ratios, while keeping constant several velocities.

locities, the force imposed at the Euler-Bernoulli beam and the force imposed at the shear beam displays only negative amplitudes. It is important to note that positive amplitudes means that there is energy being added into the system, while negative amplitudes means that energy is being absorbed out of the system.

4.2 Results Model B

Figure (4.7) illustrates the displacement under the moving load when the load is close to the transition zone (left panel) and far from it (right panel). It can be seen that the hybrid Model amplifies the response of the displacement under the moving load with increasing velocities, for sub-critical regime. Followed by a decreased of the amplification for super-critical regime. It is important to note that the top layer of springs represent the sleepers and ballast, which normally they don't change their distribution over space when the tracks change structures. For this reason, in this model no stiffness ratio is considered, and the top layer of springs is considered homogeneous

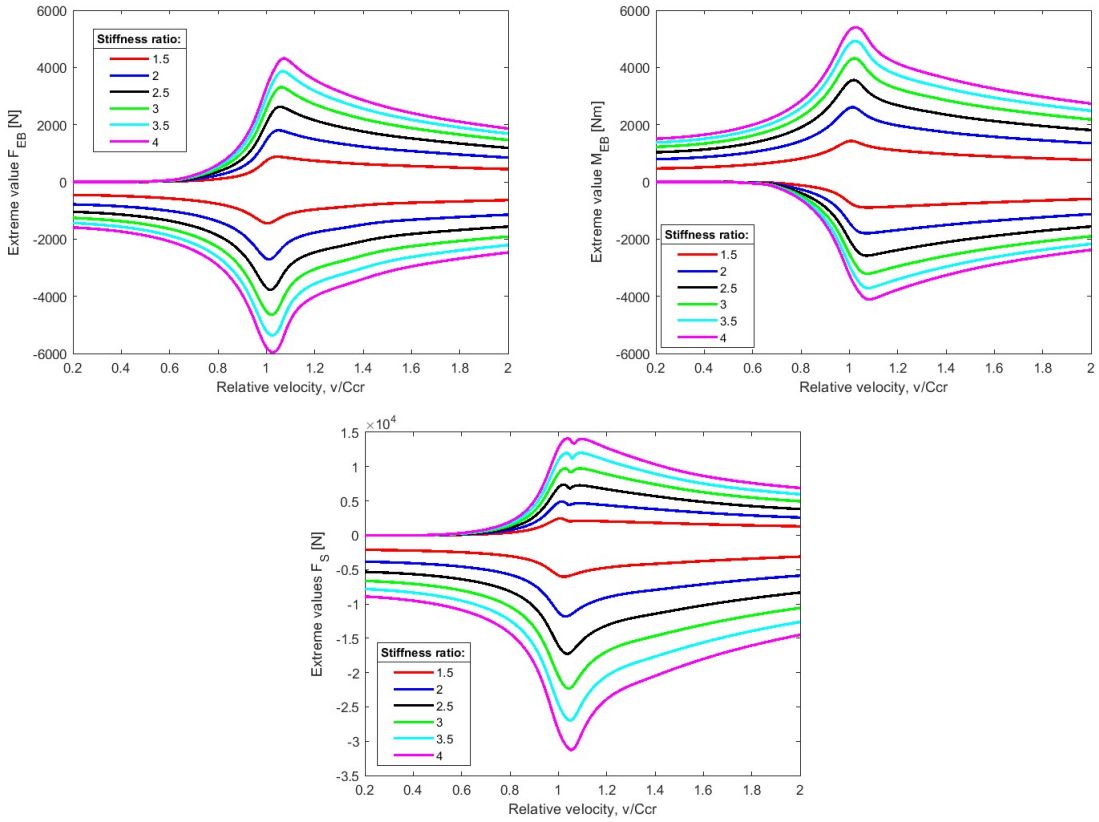

Figure 4.6: Extreme value of the active control forces and moment applied at the interface of the transition zone of Model A. Shear force imposed at Euler-Bernoulli beam (top-left panel), Moment imposed at Euler-Bernoulli beam (top-right panel), and shear force imposed at the shear beam (bottom panel).

throughout the model.

Figure (4.8) illustrates the force amplification of the transition zone along the tracks, for a system with and without the inclusion of the active control forces, when subjected to a constant moving load of 75% of the critical velocity of the system. The same is observed as in Figure (**??**), more specifically that the force amplification has been mitigated in the soft domain, for both beams, while there is an increase in the force amplifications in the rigid domain of the system, which extends to close to $10m$ after the interface of the transition zone.

The time history comparison of the behavior of the active control forces and moment are presented in Figure (4.9), for several velocities. The duration of the active control forces and moments over time exhibits a decreasing trend as the velocity of the moving load increases. Moreover, small amplitude peaks start developing as the velocity of the moving load approaches the critical velocity. Furthermore, the higher the velocity of the moving load, once these opposite sign peak pattern started, the more peaks that the active control forces and moment starts developing. Furthermore,

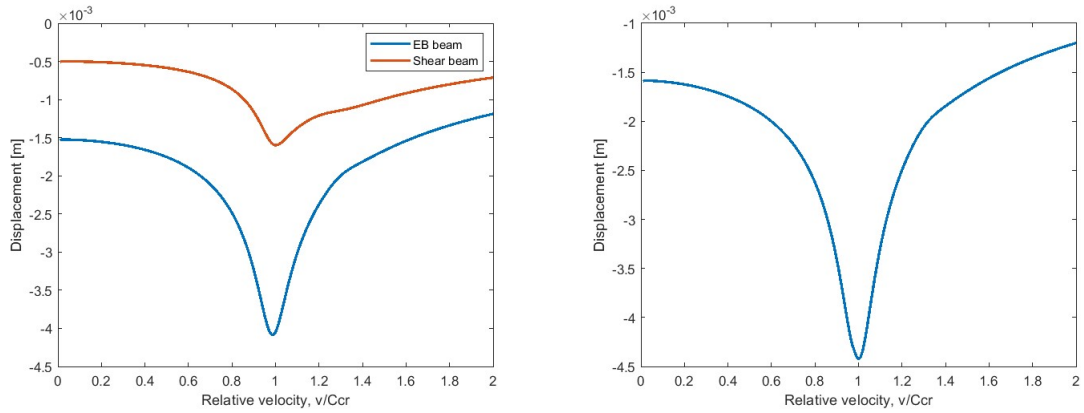

Figure 4.7: Maximum displacement under the moving load; far from the transition zone (left panel), and close to the transition zone (right panel) of Model B.

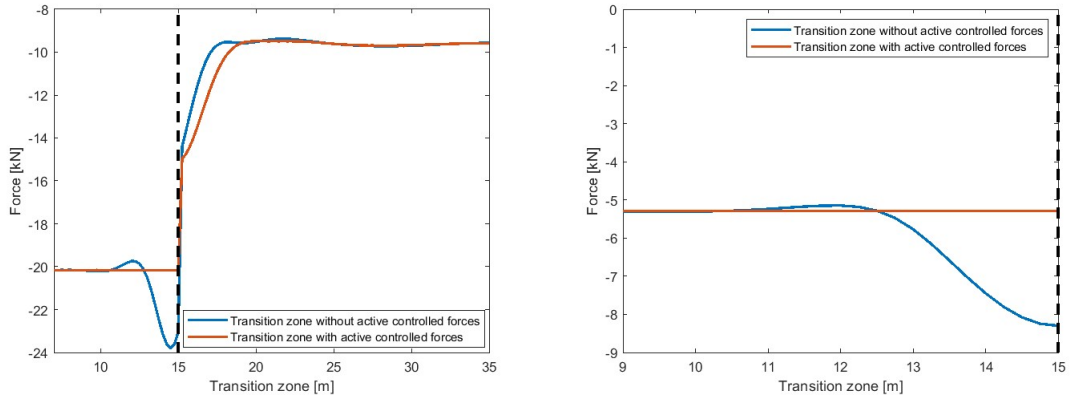

Figure 4.8: Maximum force experienced at both springs levels in the Hybrid Model. Top spring layer (left panel) and bottom spring layer (right panel).

the active control force applied at the shear beam demonstrates a different behavior than the active control force applied at the Euler-Bernoulli beam. From the lower panel of Figure (4.9), it can be seen that the active shear force imposed at the shear element exhibits a 'flipping nature', meaning that it displays two major peaks on its response over time. These two peaks have always opposite signs, and they occurs regardless of the velocity of the moving load. However, they get more pronounce with higher velocities of the moving load. Moreover, it is important to note that the time moment at which the amplitude of the interface forces changes sign does not align precisely with the time moment at which the moving load crosses over the interface of the transition zone. Instead, the change in sign occurs slightly after the moving load crosses the interface of the transition zone.

The energy required by the active control forces and moment to fully mitigate the dynamic amplification of the soft domain in the transition zone is presented in Figure (4.10). It can be seen that only the active moment applied at the Euler-Bernoulli beam adds energy into the system,

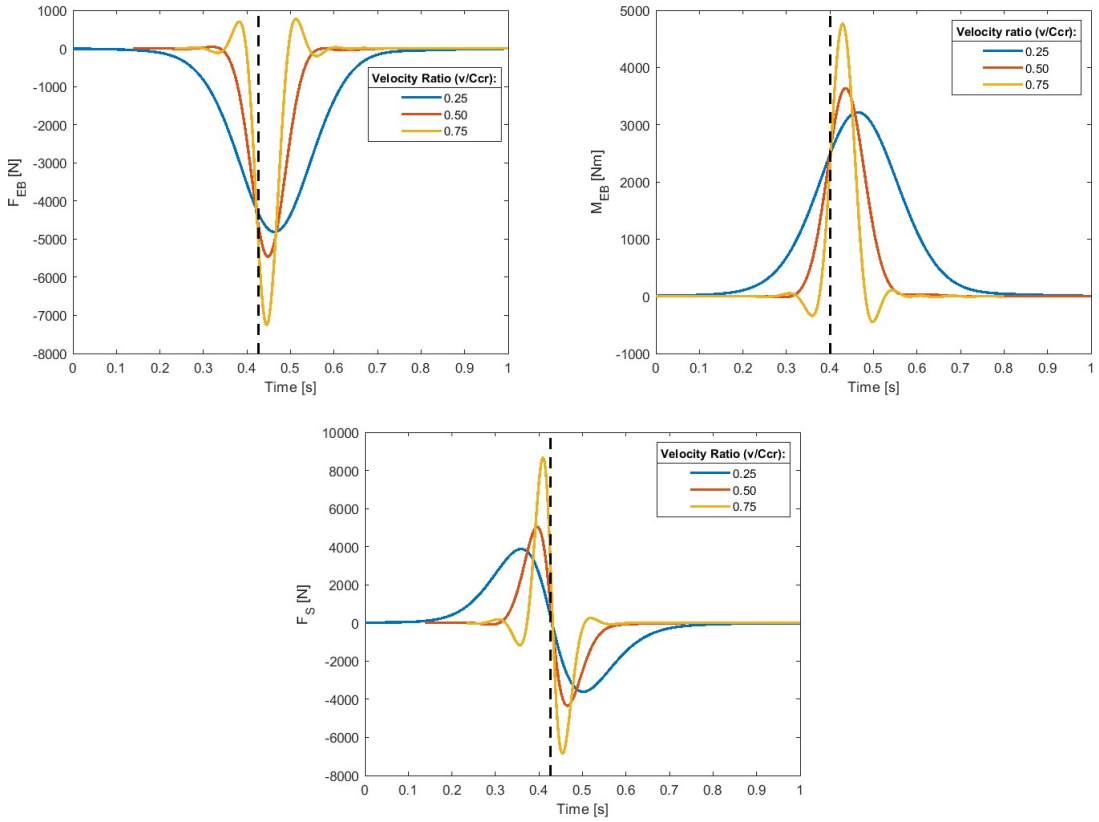

Figure 4.9: Time history comparison of the behaviour of the active control forces and moment of the Hybrid Model. The dashed line indicates the moment in time when the moving load crossed over the interface of the transition zone.

while the force acting on the Euler-Bernoulli beam and the shear beam absorbs energy out of the system. Similarly to the previous model the energy inputted/absorbed by the active control forces and moment reach a maximum at critical velocity. Moreover, regardless of the velocity of the moving load, these forces solely input or absorb energy in the system.

In Figure (4.11), the extreme amplitudes of the active control forces and moments applied at the interface of the transition zone for varying velocities are presented. It can be seen that the amplitudes of the active control forces reach a peak at critical velocity. It can be seen that the active control forces acting at the Euler-Bernoulli beam exhibit solely negative amplitudes for velocities smaller than 50% of the critical velocity, while the active moment exhibits only positive amplitudes. However, the active control force acting at the shear beam exhibits both sign amplitudes, positive and negative, but with a tendency to have higher positive amplitudes than negative.

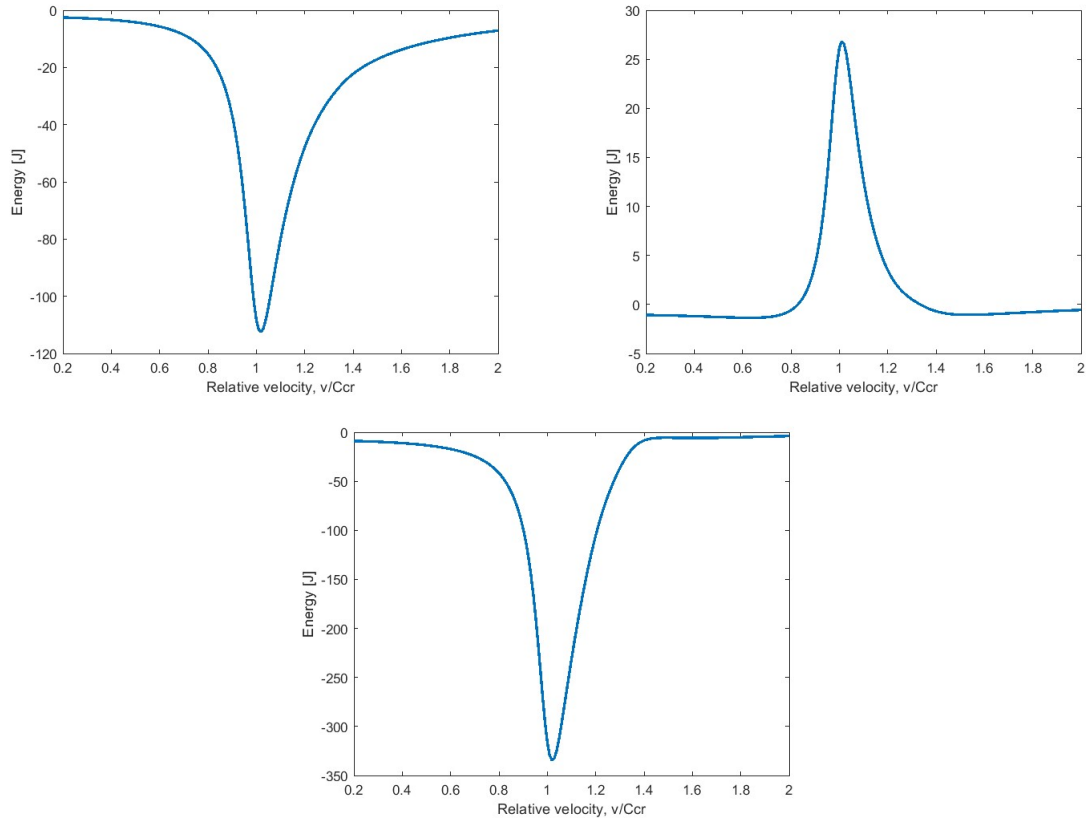

Figure 4.10: Energy required by the active control forces and moment applied at the interface of the transition zone of the Hybrid Model in order to mitigate the transient response, for varying velocities. Shear force imposed at Euler-Bernoulli beam (top-left panel), Moment imposed at Euler-Bernoulli beam (top-right panel), and shear force imposed at the shear beam (bottom panel).

4.3 Comparison Between Models and Discussion

It can be seen that both models, Model A and the Hybrid Model, amplify their response for increasing velocities (Figure (4.1) and Figure (4.7), for Model A and the Hybrid Model, respectively). When the moving load is passing over the transition zone, the system experiences amplification of the response, leading to greater displacements under the moving load just before the interface. This happens due to the difference on the vertical stiffness between both domains, on which, the higher the difference, the more pronounce the free-field becomes. This free-field interferes the eigen-field, increasing the displacement under the moving load (amplifying the response), which leads the stresses in the different components of the transition zone to increases, ultimately accelerating the degradation of them.

However, it is important to note that the amplification of the response close to the transition zone of Model A and the Hybrid Model is not identical, even if the vertical stiffness of the rigid domain

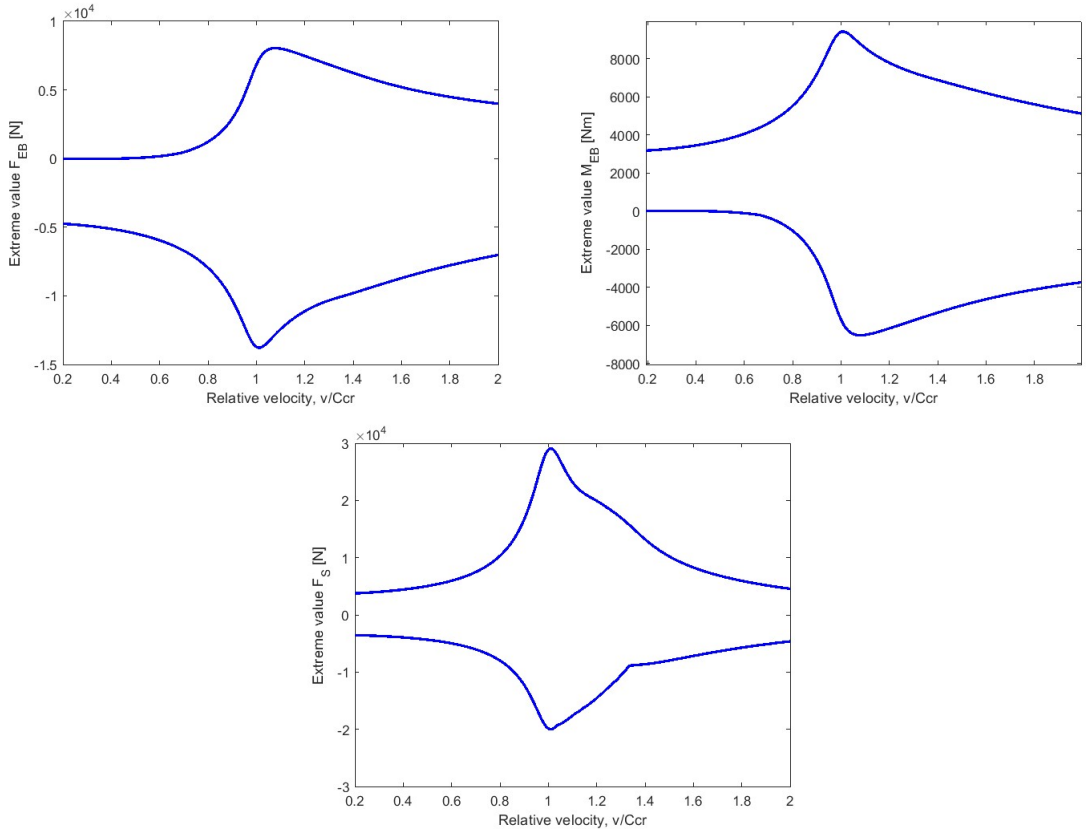

Figure 4.11: Extreme value of the active control forces and moment applied at the interface of the transition zone of Model A. Shear force imposed at Euler-Bernoulli beam (top-left panel), Moment imposed at Euler-Bernoulli beam (top-right panel), and shear force imposed at the shear beam (bottom panel).

were to be matched in both models. This disparity arises from the modeling approach employed in the Hybrid Model, where the shear beam is configured with an free end. This configuration intensifies the excitation of the free-field when the eigenfield interacts with the transition zone. In the scenario where both models were to have the same properties, the amplification of the response in the hybrid model would be greater than in Model A.

Figure (4.2) and Figure (4.8) illustrates the force amplification of the two layer of springs, along the transition zone for Model A and the Hybrid Model, respectively. It can be seen that in both models the active control forces completely mitigate the force amplification of both layer of springs in the soft domain, and that the free-field of the soft domain has completely been mitigated. However, in the stiff domain, the active control forces increases further the force amplification in the system. This means that the stresses in the different components of the transition zone in the rigid domain, increases, which would leads to this zone to degrade at a quicker pace than when the transition zone does not include active control forces.

When comparing Model A and the Hybrid Model's active control forces and moment behaviour over time, we can see several similarities on their results. The time for which the active control forces and moments are activated due to the passing load are very similar, for the same velocities of the moving load. In both models these activation time decreases with increasing velocity. This is due to the reduced time of interaction between the moving load and the transition zone, due to the quicker passage of the moving load over the transition zone. Moreover, both models also develop opposite sign peaks much smaller, in the active control forces and moments, than the main peak at the same velocity (at 50% of the critical velocity), and as the velocity of the moving load increases, their 'wavy pattern' is also the same. These additional peaks are closely related to the eigenfield response of the elements within the transition zone (Euler-Bernoulli beam and shear beam). Notably, as the velocity of the moving load increases, the eigenfield response exhibits a more pronounced 'wavy' pattern, giving rise to the observed opposite sign small peaks in the active control forces and moments.

Furthermore, in the case of the active control forces and moments imposed at the Euler-Bernoulli beam, both models reach their maximum amplitude of force and moment at the same time. However, in the case of the active control forces imposed at the shear beam, it can be seen that they react quite different. The force imposed at the shear beam in the Hybrid Model exhibits a 'flipping' nature on their amplitude over time, on which, two opposite sign, peaks are exhibited. It can also be seen that the amplitudes of the active control forces exhibited by Hybrid Model are much higher than those exhibited by Model A. This 'flipping' nature of the response of the force applied at the shear beam can be attributed to the shear beam's discontinuity in the rigid domain of the transition zone. Specifically, the waves traveling in the shear beam are reflected backward in the beam due to its boundary condition (free end), leading to a rapid sign change in the active control force to compensate for the reflected field in the shear beam. This free end of the shear beam is also the reason of the increased extreme amplitudes exhibited by the active control forces. Due to the unfixed nature of the end on the shear beam, more energy is required to restore it to its original position, and to mitigate the dynamic amplifications of the soft domain of the transition zone. Hence, the shape that the interface forces and moments takes, depend upon the interaction of both domains at the interface of the transition zone. When there is continuity in the elements over the transition zone, the active control forces and moments exhibit a profile which is similar to the eigenfield response of the system, however, when there is no continuation over the transition zone, and the elements are free to deform, the response exhibits a 'flipping' nature. This implies that there would be a sudden change in the stresses in the elements of the transition zone.

When looking at the curve of energy demands of the active control forces and moments for Model A (Figure (4.4)) and for the Hybrid Model (Figure (4.10)), there can be seen a clear similitude on the shape of the profiles. It can be seen that in both models the active control force applied at the Euler-Bernoulli beam and the active control force acting at the shear beam are responsible of absorbing energy out of the system, while the active moment applied at the Euler-Bernoulli beam adds energy into the system. In both models, it can be seen that the absorption and addition of energy, by the active control forces and moments, peak at critical velocity. Moreover, it is also important to note that overall the active control forces absorb energy out of the system, this way the dynamic amplifications in the soft domain of the transition zone can be mitigated.

When looking at the energy requirements by the active control forces vs stiffness ratio, for constant velocities in Model A (Figure (4.5)), it can be seen that there is a considerable change in the energy required to mitigate the dynamic amplifications in the soft domain of the transition zone for different velocities of the moving load. Notably, there is a modest change observed specifically

when comparing the energy required by the active control forces and moments for velocities lower than 50% of the critical velocity. However, for the other velocities, the difference in energy is even more pronounced, reaching the highest energy demands at critical velocity, and then lowering for super-critical regime.

The combined analysis of the energy requirement vs velocity of both Models (Figure (4.4) for Model A and Figure (4.10) for the Hybrid Model) and the energy demand vs stiffness ratio (Figure (4.5)) leads to the conclusion that depending upon the regime of velocity of the moving load and of the stiffness ratio, the dominating parameters in the reposes of the system differ. For relatively low velocities (up to 75% of the relative velocity), and low stiffness ratios (up to a stiffness ratio equal to 3) a 25% change in stiffness ratio leads to much more significant change in the response of the system, than a change of 25% in the relative velocity, meaning that for low stiffness ratios and velocity the system is dominated by the change in stiffness ratio. However, for higher velocities (greater than 75% of the relative velocity), it can be seen that the response of the system is dominated by the change of velocity of the moving load, where a change in 25% of the relative velocity leads to much more significant changes in the response of the system than any change in stiffness ratios. This holds until extremely high velocities have been reach (greater than 1.50% of the relative velocity), on which the system is dominated again by the change in stiffness ratio. Hence, it can be concluded that for relatively low and very high velocities of the moving load, the most influential parameter into the system is the stiffness ratio of the bottom layer of springs in the transition zone, however, for medium velocities of the moving load, the response of the system is dominated by the velocity of the moving load.

It can be seen that in both models, when looking at the active control forces on the elements which are continuous over the transition zone (all the panels of Figure (4.6) for Model A and top panels of Figure (4.11) for the Hybrid Model), that they exhibit solely either positive or negative amplitudes in their response for velocities less than 50% of the critical velocity. For these velocities, the response of the eigenfield does not develop smaller amplitude peaks, but only a single peak corresponding to the displacement under the moving load. As a result, the active control forces and moment exhibit either solely positive or negative amplitudes for such velocities. Once, the velocity increases further, these small amplitude peaks in the eigenfield start appearing, which are reflected in the behaviour of the active control forces and moments. Moreover, the behaviour of the active control force imposed at elements that are not continuous over the transition zone, as is the case of the shear beam in the Hybrid Model (bottom panel Figure (4.11)), they exhibits always positive and negative amplitudes due to the wave reflection at the transition zone, which leads to the ‘flipping ’ nature of the active control force.

Chapter 5

Conclusions and Further Studies

This chapter summarises the main findings and conclusions obtained from this study. It also gives meaningful leads on how to continue with this research, and which aspects of it could be improved.

5.1 Conclusions

The effectiveness of implementing active control forces and moments at the location of the transition between a soft to a rigid domain of a transition zone to mitigate the force amplifications of the soft domain was the main goal of this research. In response to the research question the main conclusions with respect to the implementation and behaviour of these active control forces and moments are presented as follows:

- The active control forces are capable of fully mitigating the dynamic amplification in the soft domain of transition zones. However, the active control forces leads to force amplification in the rigid domain of transition zones.
- The shape that the active control forces and moments over time takes depend upon the interface interaction between both domains of the transition zone. When the interface has continuous elements, the shape of the active forces and moment takes is similar to the eigenfield of the system. However, when the interface has discontinued elements, the shape of the active control forces and moments exhibit a 'flipping' nature.
- Of the two parameters studied (velocity and vertical stiffness), the dominating parameter in the response of the system depends upon the regime that the system is being subjected to. For relatively low and extremely high velocities of the moving load, the system is dominated by the vertical stiffness ratio, however, for medium velocities of the moving load, the system is dominated by the velocity of the moving load. Also, the duration over which the active control forces and moments are active, reduces with increasing velocities. This means that the elements that will be derived to apply these active control forces and moment must be sensitive enough to do it swiftly.
- Transition zones with discontinuous elements over their interfaces between the soft and the rigid domain, require much more energy to be absorbed and added to the system, in order to

mitigate the dynamic amplifications, than those with continuous elements over the interface of the transition zone. This must also be considered when designing transition zones, as the geometry of transition interface influences the required capabilities of the elements to be used.

To sum up, it was concluded that it is possible to diminish the dynamic amplifications in the soft domain of the transition zones, as well as lowering the amplifications in the rigid domain, by implementing active control forces and moments at the location of the transition centre, when the transition zone is subjected to a constant moving load travelling from a soft to a rigid domain, when the sensitivity of stiffness and velocities variations are taken into account. Hence, the results presented in this thesis can be used as a first step to design the passive elements that can be used to mitigate the dynamic amplifications in soft domains of transition zones, however must be kept in mind that this method amplifies the dynamic amplification at rigid domains of transition zones, and depending upon their properties (of the elements in the rigid domain of the transition zone), the performance of transition zones may be lowered.

5.2 Further Studies

Although this thesis generated new insights into how to mitigate the dynamic amplification in the soft domain of transition zones, it has its obvious limitations. For example, simplistic models have been used. There are several aspects on which this thesis could be improved. Some further studies aspects to consider are:

- The most interesting recommendation for further studies of this thesis is to design a passive control strategy that is able to show a similar level of mitigation success as the active control developed in this thesis.
- The method developed in this thesis to mitigate the dynamic amplifications in the soft domain works. However, this amplify the response in the stiff domain of transition zones. For this reason, it could be interesting to investigate a criterion for determining these active control forces, such that a balance is reach in terms of minimizing the dynamic amplifications in the soft domain of transition zones, and not increasing the dynamic amplifications in the rigid domain too much.

Bibliography

[1] Lundqvist A., R. Larsson, and T. Dahlberg. Influence of railway track stiffness variations on wheel/rail contact force. Technical report, Linköping University, 2006.

[2] C. Alves Ribeiro, A. Paixão, E. Fortunato, and R. Calçada. Under sleeper pads in transition zones at railway underpasses: numerical modelling and experimental validation. *Structure and Infrastructure Engineering*, 11(11):1432–1449, 2015.

[3] Transportation Research Board, Engineering National Academies of Sciences, and Medicine. *Design of Track Transitions*. The National Academies Press, Washington, DC, 2006.

[4] B. E. Z. Coelho. *Dynamics of railway transition zones in soft soils*. PhD thesis, Delft University of Technology, 2011.

[5] J. M. de Oliveira Barbosa, A. B. Fărăgău, and K. N. van Dalen. A lattice model for transition zones in ballasted railway tracks. *Journal of Sound and Vibration*, 494:115840, 2021.

[6] European Commission. Seventh monitoring report on the development of the rail market under article 15(4) of directive 2012/34/eu of the european parliament and of the council. Technical report, European Commission, Brussels, Belgium, 2021.

[7] A. B. Fărăgău. *Understanding degradation mechanisms at railway transition zones using phenomenological models*. PhD thesis, Delft University of Technology, 2023.

[8] A. B. Fărăgău, C. Keijdener, J. M. de Oliveira Barbosa, A. V. Metrikine, and K. N. van Dalen. Transition radiation in a nonlinear and infinite one-dimensional structure: a comparison of solution methods. *Nonlinear Dynamics*, 103(2):1365–1391, 1 2021.

[9] A. B. Fărăgău, T. Mazilu, A. V. Metrikine, T. Lu, and K. N. vanDalen. Transition radiation in an infinite one-dimensional structure interacting with a moving oscillator—the green's function method. *Journal of Sound and Vibration*, 492:115804, 2021.

[10] A. B. Fărăgău, A. V. Metrikine, and K. N. van Dalen. Transition radiation in a piecewise-linear and infinite one-dimensional structure–a laplace transform method. *Nonlinear Dynamics*, 98(4):2435–2461, 12 2019.

[11] H. Heydari-Noghabi, J. N. Varandas, M. Esmaeili, and J. Zakeri. Investigating the influence of auxiliary rails on dynamic behavior of railway transition zone by a 3d train-track interaction model. *Latin American Journal of Solids and Structures*, 14(11):2000–2018, 2017.

[12] G. A. Hunt. Review of the effect of track stiffness on track performance. Technical report, Rail Safety Standards Board, 2005.

[13] B. Indraratna, M. Babar Sajjad, T. Ngo, A. Gomes Correia, and R. Kelly. Improved performance of ballasted tracks at transition zones: A review of experimental and modelling approaches. *Transportation Geotechnics*, 21:100260, 2019.

[14] R. Insa, P. Salvador, J. Inarejos, and A. Roda. Analysis of the influence of under sleeper pads on the railway vehicle/track dynamic interaction in transition zones. *Proceedings of the Institution of Mechanical Engineers, Part F: Journal of Rail and Rapid Transit*, 226(4):409–420, 2012.

[15] G. Jing, Q. Luo, Z. Wang, and Y. Shen. 1526. micro-analysis of hanging sleeper dynamic interactions with ballast bed. *Journal of Vibroengineering*, 17:444–454, 2015.

[16] B. Jouna. On the efficiency of mitigation measures in reducing the amplified response at transition zones in railway tracks: tuned mass dampers, auxiliary rails, and under-sleep pads, 2022.

[17] A. D. Kerr and L. A. Bathurst. Method for upgrading the performance at track transitions for high-speed service : next generation high-speed rail program. Technical report, Federal Railroad Administration, 2001.

[18] M. Labrado Palomo, F. Roca Barceló, F. Ribes Llario, and J. Real Herráiz. Effect of vehicle speed on the dynamics of track transitions. *Journal of Vibration and Control*, 24(21):5118–5128, 2018.

[19] A. Lundqvist and T. Dahlberg. Load impact on railway track due to unsupported sleepers. *Proceedings of the Institution of Mechanical Engineers, Part F: Journal of Rail and Rapid Transit*, 219(2):67–77, 2005.

[20] P. Meijers and P. Holscher. Lasting flat raods and railways: Literaturestudy of knowledge and experience of transition zones. Technical report, Delft University of Technology, 2007.

[21] J. Nasarre. Transiciones obra de paso-terraplén: los bloques técnicos en las vías ferroviarias. proyecto y conservacíon. Technical report, Fundacion Caminos de Hierro, 2007.

[22] A. Paixão, C. Alves Ribeiro, N. Pinto, E. Fortunato, and R. Calçada. On the use of under sleeper pads in transition zones at railway underpasses: experimental field testing. *Structure and Infrastructure Engineering*, 11(2):112–128, 2015.

[23] A. Paixão, E. Fortunato, and R. Calçada. Transition zones to railway bridges: Track measurements and numerical modelling. *Engineering Structures*, 80:435–443, 2014.

[24] A. Paixão, E. Fortunato, and R. Calçada. A numerical study on the influence of backfill settlements in the train/track interaction at transition zones to railway bridges. *Proceedings of the Institution of Mechanical Engineers, Part F: Journal of Rail and Rapid Transit*, 230(3):866–878, 2016.

[25] A. Paixão, J. N. Varandas, E. Fortunato, and R. Calçada. Numerical simulations to improve the use of under sleeper pads at transition zones to railway bridges. *Engineering Structures*, 164:169–182, 2018.

[26] R. Sañudo, L. dell'Olio, J.A. Casado, I.A. Carrascal, and S. Diego. Track transitions in railways: A review. *Construction and Building Materials*, 112:140–157, 2016.

[27] I. Seara and A. Gomes Correia. Transition zones of railways. the importance of a geostructural solution. Technical report, Universidade do Minho, 2008.

[28] M. Shahraki, C. Warnakulasooriya, and K. J. Witt. Numerical study of transition zone between ballasted and ballastless railway track. *Transportation Geotechnics*, 3:58–67, 2015.

[29] M. Shahraki and K. J. Witt. 3d modeling of transition zone between ballasted and ballastless high-speed railway track. *Journal of Traffic and Transportation Engineering*, 3, 04 2015.

[30] M. Sysyn, O. Nabochenko, and V. Kovalchuk. Experimental investigation of the dynamic behavior of railway track with sleeper voids. *Railway Engineering Science*, 28(3):290–304, 9 2020.

[31] X. Xiao, Y. Li, T. Zhong, and X. Sheng. Theoretical investigation into the effect of rail vibration dampers on the dynamical behaviour of a high-speed railway track. *Journal of Zhejiang University-SCIENCE A*, 18(8):631–647, 8 2017.

[32] T. Xin, Y. Ding, P. Wang, and L. Gao. Application of rubber mats in transition zone between two different slab tracks in high-speed railway. *Construction and Building Materials*, 243:118219, 2020.

[33] Bezin Y., S. D. Iwnicki, M. Cavalletti, E. de Vries, F. Shahzad, and G. Evans. An investigation of sleeper voids using a flexible track model integrated with railway multi-body dynamics. *Proceedings of the Institution of Mechanical Engineers, Part F: Journal of Rail and Rapid Transit*, 223(6):597–607, 2009.

[34] J. Y. Zhu, D. J. Thompson, and C. J. C. Jones. On the effect of unsupported sleepers on the dynamic behaviour of a railway track. *Vehicle System Dynamics*, 49(9):1389–1408, 2011.